RF manipulations of high-intensity hadron beams in SIS-100

Yao-Shuo Yuan[1], Oliver Boine-Frankenheim[1,2], Thilo Egenolf[2] and Vladimir Kornilov[2]
[1] Technische Universität Darmstadt, Schlossgartenstr. 8, 64289 Darmstadt, Germany
[2] GSI Helmholtzzentrum für Schwerionenforschung GmbH,
Planckstrasse 1, 64291 Darmstadt, Germany

November 5, 2021

Abstract

The international accelerator facility for high-intensity hadron beams FAIR is under construction at GSI Darmstadt in Germany. In order to fulfill the users requests, schemes of manipulations of proton beams and heavy ion beams, consisting of longitudinal bunch merging and batch compression are proposed for the main synchrotron SIS100. The intensity effects, mainly longitudinal space charge and the cavity beam loading, can cause beam collective oscillation and emittance growth. In this report, longitudinal manipulations of proton beams and heavy ion (U^{28+}) beams affected by space charge and by beam loading are investigated. Schemes for the space charge and beam loading compensation to reduce the emittance growth are presented.

Contents

1 Introduction

In the past few years, several projects of high-intensity hadron (proton or ion) synchrotrons were proposed or under construction, to satisfy the increasing demand of short and intense bunches for many applications. Efficient schemes to compress bunched beams and thus to improve beam intensity are of practical concerned. For the FAIR project, a scheme of longitudinal manipulations is recently proposed to compress hadron beams for the future synchrotron SIS100 [1, 2, 3]. It includes a sequence of bunch merging, bunch"batch compression", and a fast bunch compression, as well as a fast bunch rotation for heavy ion beams [4].

The principle of bunch merging is to perform longitudinal merging pairs of two bunches without longitudinal phase space dilution by adiabatically adjusting rf voltage with different harmonic numbers. It can be achieved via decreasing the amplitude of rf voltage on initial harmonics and simultaneously increasing the one on the halved harmonics. It should be noted that the phrase "adiabatic" here refers to the rf voltage change slowly so that the longitudinal beam behavior can be reversible, which is defined in different way as defined in thermodynamics, where adiabaticity means the preservation of the intrinsic energy. Compared to the conventional de-bunching and re-bunching method, the bunch-merging scheme has several advantages. Firstly, for an ideal (adiabatic) bunch merging, the longitudinal emittance remains constant with negligible phase space dilution. Secondly, the beams are always focused within buckets as bunches during bunch merging. In comparison, during de-bunching (or re-bunching) process, the drifting beam is left uncontrolled and the full ring filled with particles [5]. The bunch merging scheme, since initially proposed in 1983 [6], has been successfully applied on several accelerator machines, for example on the CERN-PS for the production of anti-proton beam [5, 7], as well as on the RHIC for generating one single bunch [8, 9]. Batch compression is a process in which the number of bunches keeps constant while the "batch of the bunches" is concentrated in a reduced fraction of the accelerator circumference [7, 10, 11]. It can be achieved via slowly (adiabatically) decreasing of the rf voltage amplitude on lower harmonic while simultaneously increasing the one on the higher harmonic. During batch compression, bunched beams can be "handed over" from the lower harmonic to the higher one. The whole batch is compressed by a factor of the ratio of the two harmonic numbers. After several repetition of the above process, large compression factor can be obtained. The fast bunch compression, achieved via a 90° non-adiabatic fast rotation in mismatched rf bucket in longitudinal phase space, will be used in SIS100 to further compress the heavy ion bunch before fast exaction.

For high-intensity hadron beams, longitudinal intensity effects, mainly referring to effects of longitudinal space charge (hereafter called space charge for short) and cavity beam loading (hereafter called beam loading for short), are of concerned and should be treated carefully to avoid beam quality deterioration, as the beam intensity is being enhanced during such longitudinal manipulations. Specifically, below the transition energy the space-charge-induced voltage inside the bunched beam can weaken the effective rf voltage acting on the beam, while beam loading can induce wakefields in an rf cavity, causing beam oscillation or even beam instabilities [12].

As an introductory example, the proposed manipulation schemes for proton bunch in SIS100 are shown in Fig. 1. It consists of three stages. Firstly, four adjacent bunches in ten harmonics are merged into two bunches, with harmonic number decreasing gradually from 10 to 5. Secondly, the two bunches "concentrate" via increasing the harmonic numbers from 5 to 10 step by step (so called "batch compression"). Finally, the two shrunk bunches are merged again into one single bunch. The relevant bunch parameters are listed in Tab. 1.

In the present report, we investigate the beam behavior in the presence of intensity effects during the RF manipulations of proton and heavy ion bunches in SIS100, aiming at proposing optimized schemes to compensate intensity effects. The effects of beam loading and space charge

Table 1: Example parameters for the scenario of proton bunch longitudinal manipulation in SIS100.

Parameter [unit]	Symbol	Value
Atomic mass	A	1.0
Charge state	Z	1.0
Kinetic energy [GeV/u]	E_k	4.0
Intensity per bunch	N	5.0×10^{12}
Slip factor	η	-0.0238
Initial bare synchrotron tune	Q_{s0}	8.0×10^{-4}
Initial rms bunch length [m]	$\tilde{z}_m$	6.26
Initial rms momentum spread	$\tilde{\delta}_z$	1.10×10^{-3}

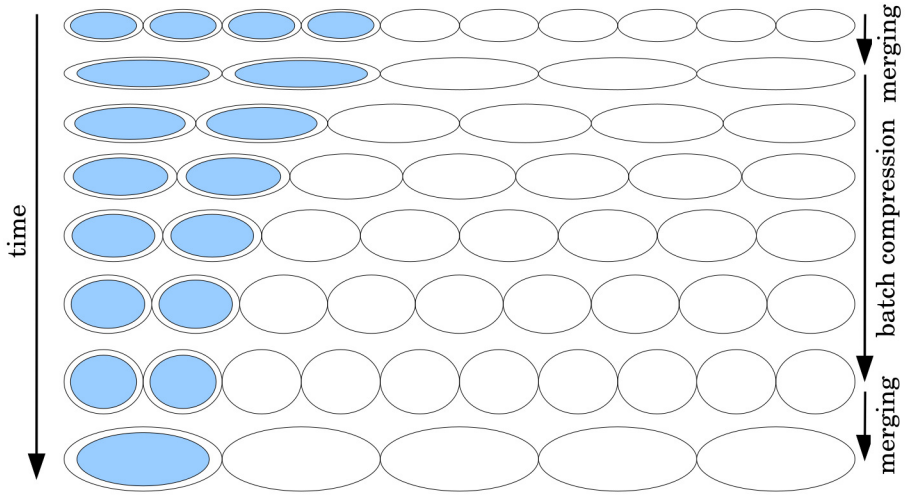

Figure 1: Proposed RF manipulation scheme for the proton bunches in SIS100

are numerically calculated and the particle-in-cell (PIC) simulations are performed. The report is organized as follows. Fundamentals of longitudinal beam dynamics are presented in Sec.2. From Sec. 3 to Sec.7, proton bunch merging and batch compression with space charge and beam loading effect are separately analyzed in detail. An optimized example of the longitudinal manipulation of proton bunch is shown in Sec. 8. In Sec.9 the scheme for heavy ion bunch manipulation including fast bunch rotation is proposed. Finally, a summary is given in Sec.10.

2 Longitudinal beam dynamics

2.1 Basic equations

The longitudinal equation set of motion for a single particle reads (see, for example, Ref. [13])

$$\dot{\phi} = h\omega_0\eta\delta, \tag{1}$$

$$\dot{\delta} = \frac{\omega_0}{2\pi\beta^2 E} q\Delta V. \tag{2}$$

Here, the phase space coordinates (ϕ, δ) denote the rf phase angle and the momentum spread of the particle, respectively; h the harmonic number; ω_0 the revolution frequency; η the slip factor; β

and E are the relative speed and the energy of the synchronous particle, respectively; $q\Delta V$ is the obtained energy difference between the single particle and the synchronous particle.

Since the bunch merging and batch compression are performed on multiple harmonics, it is more convenient to adopt the (z, v) coordinate, with z and v defined respectively as the derivation in position and in velocity from the synchronous particle

$$z \equiv \frac{R(\phi - \phi_s)}{h}, \qquad v \equiv \dot{z}. \tag{3}$$

Here, R is the average radius of the synchrotron, and the symbol "$\cdot$" represents the derivative with respect to time. From Eq. 1, Eq. 2 and Eq. 3 one can find $v = \eta\beta c\delta$, with c the speed of light. The equation set of motion Eq. 1 and Eq. 2 can be rewritten in the (z, v) coordinate as

$$\dot{z} = v, \tag{4}$$

$$\dot{v} = \frac{q\Delta V}{m^* L}, \tag{5}$$

in which the effective mass $m^* = -\gamma_0 m/\eta$ with γ_0 the relativistic parameter, $L = 2\pi R$ the circumference of the ring. Clearly, Eq. 4 and Eq. 5 can be derived from the corresponding Hamiltonian

$$H = \frac{v^2}{2} + \frac{qV_0}{m^* L} Y(z), \tag{6}$$

with the normalized "energy potential" defined as

$$Y(z) = \frac{1}{V_0} \int_0^z V(z) dz. \tag{7}$$

Here V_0 and $V(z)$ is the amplitude and the profile of the voltage, respectively.

In the presence of space charge, $V(z)$ can be divided into the external rf voltage part V_{rf} and longitudinal space charge voltage part V_{sc}, with its expression (see, e.g., Ref. [13, 14])

$$V_{\mathrm{sc}} = -q\beta c R X_{\mathrm{sc}} \frac{\partial \lambda}{\partial z}, \tag{8}$$

in which λ represents the line density of the bunch, and X_{sc} the space charge reactance

$$X_{\mathrm{sc}} = \frac{g}{2\epsilon_0 \beta c \gamma^2}, \tag{9}$$

with the g-factor $g = 1 + 2\ln(b/a)$ (b is the pipe radius and a the beam radius, see, e.g. Ref [14]). The energy potential of space charge can be accordingly written as

$$Y_{\mathrm{sc}} = \frac{1}{V_0} \int_0^z V_{\mathrm{sc}} dz = q\beta_0 c \frac{R X_{\mathrm{sc}}}{V_0} (\lambda_0 - \lambda), \tag{10}$$

with λ_0 denotes the line density at $z = 0$.

2.2 Elliptical bunch model

The elliptic bunch model are widely employed to deal with the longitudinal beam dynamics with space charge in a self-consistent manner. The particle distribution in an ellipse bunch model can be written as [15]

$$g(H) = c_1 \sqrt{H_m - H}, \tag{11}$$

with

$$H_m = \frac{v_m^2}{2} = -\frac{qV_0}{m^* L} Y(z_{m2}), \tag{12}$$

and

$$v_m = \eta \beta c \delta_m. \tag{13}$$

Here, v_m and δ_m are the maximum velocity and momentum spread of the particles in the bunch. $Y(z_{m2})$ is the energy potential of the particle at one end of the bunch.

The line density of the bunch can be written as [15, 16]

$$\lambda(z) = \frac{N}{u_m}[Y_{\mathrm{rf}}(z) - Y_{\mathrm{rf}}(z_{m2})], \tag{14}$$

with the coefficient

$$u_m = \int_{z_{m1}}^{z_{m2}} [Y_{\mathrm{rf}}(z) - Y_{\mathrm{rf}}(z_{m2})] dz, \tag{15}$$

and N the number of particles in the bunch.

Combining Eq. 10, Eq. 14 and Eq. 15, we have

$$Y_{\mathrm{sc}}(z) = -q\beta c \frac{RX_s}{V_0} \frac{N}{u_m} Y_{\mathrm{rf}}(z). \tag{16}$$

It can be seen from Eq. 16 that for the elliptical bunch model, the space charge potential is proportional to the external rf potential. If we define the *space charge voltage amplitude* as

$$V_{\mathrm{sc0}} = q\beta c R X_s \frac{N}{u_m}, \tag{17}$$

the total energy potential in Eq. 7 can be simplified to

$$Y(z) = Y_{\mathrm{rf}}(1 + \frac{V_{\mathrm{sc0}}}{V_0}). \tag{18}$$

Here, the sign of the space charge voltage amplitude V_{sc0} is set so as to have the same sign as V_0. Eq. 18 indicates the linearity of the longitudinal space charge in an elliptical bunch model.

The matched external rf voltage amplitude of an elliptical bunch model can be obtained from Eq. 12 and Eq. 13

$$V_{\mathrm{rf0}} = -\frac{Lm^* v_m^2}{2qY_{\mathrm{rf}}(z_{m2})}. \tag{19}$$

The space charge voltage amplitude can be calculated from Eq. 17. Thus the matched external voltage amplitude in the presence of space charge can be obtained via the linear combination

$$V_{\mathrm{rf0,sc0}} = V_{\mathrm{rf0}} + V_{\mathrm{sc0}} = -\frac{Lm^* v_m^2}{2qY_{\mathrm{rf}}(z_{m2})}(1 + \Sigma_{\mathrm{sc}}), \tag{20}$$

with

$$\Sigma_{\mathrm{sc}} = \frac{V_{\mathrm{sc0}}}{V_{\mathrm{rf0}}}, \tag{21}$$

defined as the space charge parameter [16].

2.3 Expressions in multi-harmonics rf system

For a multi-harmonic system with sinusoidal rf voltage waveform, the rf voltage acting on the particles at the position of ϕ can be separated into the part in the fundamental harmonic

$$V^{(0)}(\phi) = V_0^{(0)}(\sin\phi - \sin\phi_{\rm s}), \tag{22}$$

and the part in the $n^{\rm th}$ harmonic

$$V^{(n)}(\phi) = V_0^{(n)}\big\{\sin[\phi_{\rm s,n} + h(\phi-\phi_{\rm s}) + \phi_n] - \sin\phi_{\rm s,n}\big\}. \tag{23}$$

Here, the superscript "(n)" represents the index of the harmonic. $h = h_n/h_0$ the ratio of the two harmonic numbers. $\phi_{\rm s}$ and $\phi_{\rm s,n}$ denotes the synchrotron phases in the harmonics h_0 and h_n, respectively. ϕ_n is the phase shift between the harmonics. The corresponding normalized energy potential in Eq. 7 becomes

$$Y(\phi) = Y^{(0)}(\phi) + Y^{(n)}(\phi), \tag{24}$$

with

$$Y^{(0)}(\phi) = \cos\phi - \cos\phi_{\rm s} + (\phi-\phi_{\rm s})\sin\phi_{\rm s}, \tag{25}$$

and

$$\begin{aligned} Y^{(n)}(\phi) = \frac{r}{h}\big\{&\sin\phi_{\rm s,n} - \cos[\phi_{\rm s,n} + h(\phi-\phi_{\rm s}) + \phi_n] \\ &- h(\phi-\phi_{\rm s})\sin\phi_{\rm s,n}\big\}. \end{aligned} \tag{26}$$

Here, $r = V_0^{(n)}/V_0^{(0)}$ the ratio of rf voltage. For convenience, the synchrotron phases $\phi_{\rm s}$ and $\phi_{\rm s,n}$ are set to be zero without acceleration. The voltage amplitude $V_0^{(n)}$, and the relative phase shift ϕ_n are two essential quantities during bunch longitudinal manipulation, which will be discussed in detail in the following text.

3 Bunch merging without intensity effects

For an ideal (adiabatic) bunch merging, according to Liouville's theorem the conservation of longitudinal emittance before and after bunch merging reads

$$2\tilde{\varepsilon}_{\rm i} = \tilde{\varepsilon}_{\rm sum,f}, \tag{27}$$

with the total rms longitudinal emittance of the two merging bunches, defined by

$$\tilde{\varepsilon}_{\rm sum} = \sum_{j=1}^{2N}\sqrt{\langle z_j^2\rangle\langle\delta_j^2\rangle - \langle z_j\delta_j\rangle^2}, \tag{28}$$

and the rms longitudinal emittance for each bunch

$$\tilde{\varepsilon} = \sum_{j=1}^{N}\sqrt{\langle z_j^2\rangle\langle\delta_j^2\rangle - \langle z_j\delta_j\rangle^2}. \tag{29}$$

Here we assume that the two merging bunches are identical. N the number of particles in a bunch. The subscripts "i", "f" denote respectively the initial and final stage of the bunch merging. Clearly, Eq. 27 holds only at the beginning and at the end of bunch merging, where the rms emittance can be expressed via

$$\tilde{\varepsilon} = \tilde{z}_m\tilde{\delta}_m, \tag{30}$$

as bunches take a regular upright elliptical shape in longitudinal phase space. During the merging process, we have $\tilde{\varepsilon}_{\rm sum} > 2\tilde{\varepsilon}$.

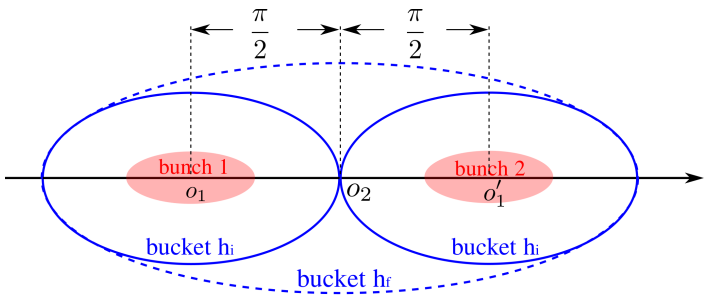

Figure 2: Schematic drawing of the relative positions of the buckets (blue) and bunches (red), as well as the phase shifts between initial h_i (solid line) and final h_f (dashed line) harmonics for bunch merging.

3.1 Required RF voltage and phase shift

In order to achieve an ideal merging, the external focusing rf voltages should be designed to be matched to bunch parameters (length and momentum spread). With given initial and final bunch parameters, the matched rf voltage at the initial and the end of the merging can be calculated based on the elliptical bunch model. During bunch merging the rf voltage amplitude should vary sufficiently slowly to always get matched to the beam parameters.

For an rf cavity with sinusoidal voltage waveforms, the rf potential and the matched rf voltage amplitude in Eq. 22 becomes

$$Y_{\rm rf}(z) = \frac{R}{h}\big[\cos(\frac{hz}{R}) - 1\big] \approx -\frac{1}{2}\frac{h}{R}z^2, \tag{31}$$

and

$$V_{\rm rf0} = \frac{L\gamma_0 m|\eta|R\beta^2c^2}{qh}(\frac{\delta_m}{z_m})^2. \tag{32}$$

Here we assume $\phi_{\rm s} = 0$ as there is no acceleration during bunch merging, and adopt the small amplitude approximation, since usually the bunch length is typically much shorter than the wave length of the rf cavity. And δ_m and z_m is the (half) bunch length and maximum momentum spread, respectively. For an elliptical bunch, we have $\delta_m = \sqrt{5}\tilde{\delta}_m$, and $z_m = \sqrt{5}\tilde{z}_m$, with the symbol "~" denotes the corresponding rms value. Eq. 32 can be employed to calculate the matched rf voltage amplitude.

Another key parameter for bunch merging is the relative phase shift between the two harmonics. Appropriate rf phase settings can avoid bunch center oscillation (dipole oscillation) and thus minimize the emittance growth during bunch merging. To this end, the phase shift should be set in such a way that the two bunches can be merged symmetrically under the combined longitudinal focusing in two harmonics. As shown schematically in Fig. 2, in order to keep the bunch merging process to be symmetrical, the relative rf phase between the initial harmonic h_i and the final harmonic h_f ($h_i = 2h_f$) in SIS 100 is set to be $\pi/2$.

3.2 Bunch merging with constant bunching factor

It can be seen from Eq. 32 that the final bunch length and momentum spread after merging is determined via the final matched rf voltage. Clearly, a higher rf voltage can generate a shorter final bunch length. Bunch merging with constant bunching factor is a desired scenario. The bunching

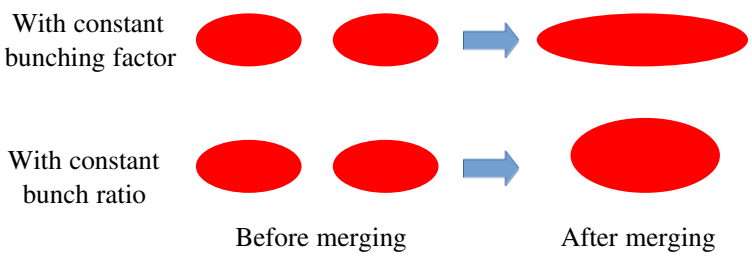

Figure 3: Schematic drawing of the comparison of bunch merging with constant bunching factor (upper) and with constant bunch ratio (lower).

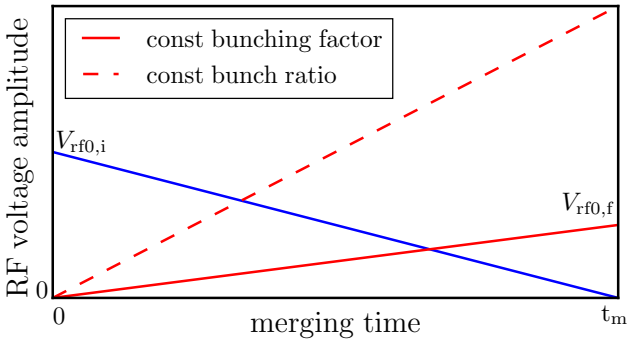

Figure 4: Schematic curves of rf voltage amplitude ramps for bunch merging on the initial (blue) and final (red) harmonic under constant bunching factor, compared with the case under constant bunch ratio (dashed).

factor is defined as the length ratio of the bunch to the bucket (see, for example, in Ref. [13]). The constant bunching factor reads

$$\frac{z_{m,i}}{l_i} = \frac{z_{m,f}}{l_f} \tag{33}$$

where l represents the bucket length. In the absence of acceleration, we have $l = L/h$.

The advantage of keeping a constant bunching factor during bunch merging lies in the fact that it can lead to a long final bunch length, using a low rf voltage, and thus results in a small transverse tune shift, avoiding potential beam transverse resonances. To illustrate this, let us compare the bunch merging under constant bunching factor and that under constant bunch ratio [6], which is defined as the ratio of the bunch length to the bunch momentum spread,

$$\frac{\delta_{m,i}}{z_{m,i}} = \frac{\delta_{m,f}}{z_{m,f}}. \tag{34}$$

Substituting Eq. 33 and Eq. 34 into Eq. 30 and Eq. 32, and taking into account emittance conservation in Eq. 27, one can easily find the following relations before and after bunch merging,

$$\delta_i = \delta_f, \quad 2z_{m,i} = z_{m,f}, \quad V_{\mathrm{rf0,i}} = 2V_{\mathrm{rf0,f}} \tag{35}$$

for constant bunching factor, and

$$\sqrt{2}\delta_i = \delta_f, \quad \sqrt{2}z_{m,i} = z_{m,f}, \quad 2V_{\mathrm{rf0,i}} = V_{\mathrm{rf0,f}} \tag{36}$$

for constant bunch ratio. A schematic comparison of the bunch merging under constant bunching factor and bunch ratio as well as the corresponding rf voltage ramps can be found in Fig. 3 and Fig. 4, whihc illustrates that with constant bunching factor the final bunch length is longer and the rf voltage amplitude is lower.

4 Bunch merging affected by space charge

4.1 Space charge matching

Let us now consider the bunch merging in the presence of (longitudinal) space charge effect. For a given bunch length, the external rf voltage should be increased to compensate the space charge defocusing effect (space charge matching). Based on the elliptical model, the coefficient u_m in Eq. 15 for a sinusoidal rf voltage waveform takes the form

$$u_m = \frac{2h}{3R} z_m^3. \tag{37}$$

Substituting Eq. 37 into Eq. 16 and Eq. 17 one can obtain the explicit expression of space charge voltage amplitude,

$$V_{\mathrm{sc0}} = \frac{3q\beta c X_s N R^2}{2h z_m^3}. \tag{38}$$

Taking Eq. 35 and Eq. 36 into account, one can find the relation of space charge voltage at the beginning and at the end of a bunch merging with constant bunching factor,

$$V_{\mathrm{sc0,i}} = 2V_{\mathrm{sc0,f}}. \tag{39}$$

Finally, the matched external voltage amplitude in the presence of space charge on the initial harmonic h_i and on the final harmonic h_f can be written as a linear summation of the matched rf voltage and the space charge voltage

$$V_{\mathrm{rf0,sc0,i}} = V_{\mathrm{rf0,i}} + V_{\mathrm{sc0,i}} \tag{40}$$

and

$$V_{\mathrm{rf0,sc0,f}} = V_{\mathrm{rf0,f}} + V_{\mathrm{sc0,f}} = 0.5 V_{\mathrm{rf0,sc0,i}}. \tag{41}$$

Here, V_{rf0} and V_{sc0} are respectively the initial matched external rf voltage amplitude and the space charge voltage amplitude.

4.2 Simulation results

A simulation example of proton bunch merging with constant bunching factor in SIS100 is performed using the particle tracking code pyORBIT [17, 18]. Based on the parameters listed in Tab. 1, the matched rf voltages are calculated via Eq. 39, Eq. 40 and Eq. 41 and listed in Tab. 2. The voltage ramps for the fundamental (initial) harmonics $h_i = h_{10}$ and for the final harmonic $h_f = h_5$ are set to be linear during bunch merging, as shown in Fig. 5. The red curve indicates the case without space charge, and the blue represents the increased external rf voltage for space charge matching. In the simulation, four identical bunches with parabolic particle distribution in four adjacent buckets in harmonic h_{10} are merged into two bunches in harmonic h_5. The particle-in-cell (PIC) scheme in the code pyORBIT is adopted for the longitudinal space charge calculation.

A practical consideration of the bunch merging is the choice of an optimum merging time. Clearly, a shorter merging time can ensure a better bunch merging with less emittance growth,

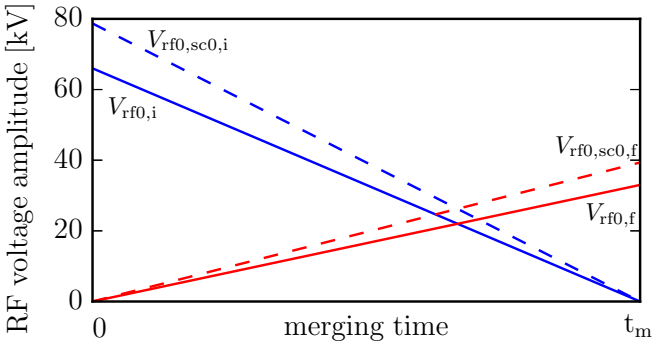

Figure 5: Proposed rf voltage amplitude ramps for h_{10} (blue) and h_5 (red) with (dashed line) and without (solid line) space charge during the bunch merging in SIS100.

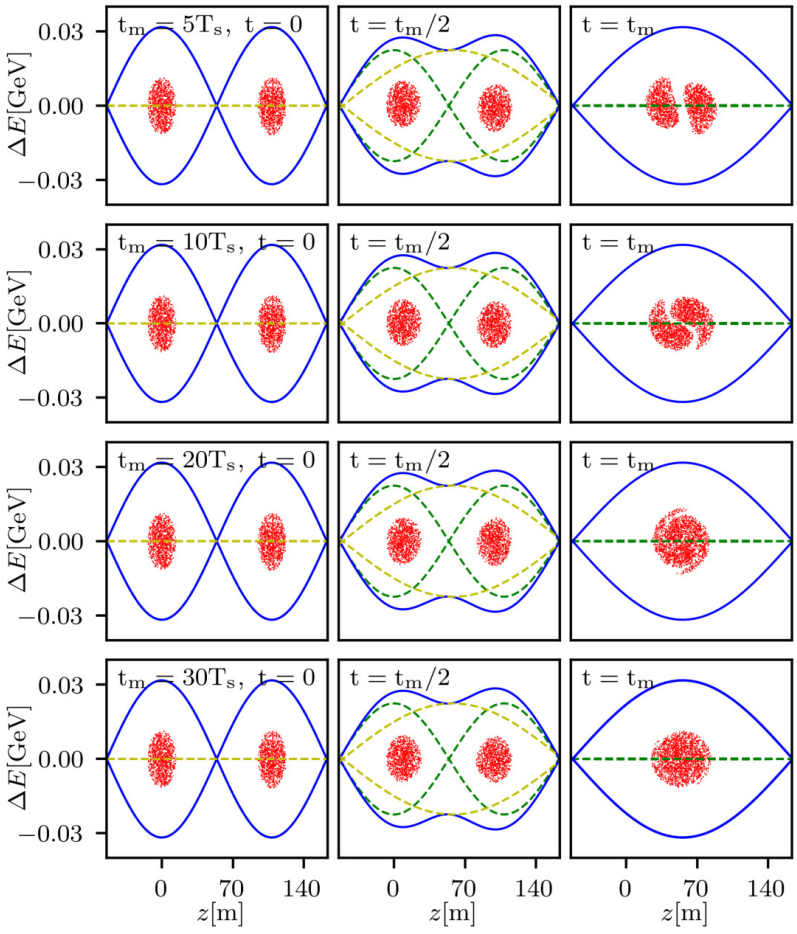

Figure 6: Particle distribution in the longitudinal phase space at initial ($t = 0$), half ($t = t_m/2$) and final ($t = \mathrm{t_m}$) during bunch merging under different merging time in the absence of space charge. The blue curve denotes the separatrix orbit of the combined harmonics of h_{10} and h_5, the green curve the separatrix orbit of the harmonic $h_{10} = 10$, and the yellow the one of the harmonic $h_5 = 5$.

Table 2: Relevant parameters of space charge matching at the initial and final of the proton bunch merging in SIS100.

Parameter [unit]	Symbol	Initial value	Final value
matched rf voltage [kv]	V_{rf0}	66.0	33.0
space charge voltage [kV]	V_{sc0}	12.7	6.35
matched rf voltage with s.c.[kV]	$V_{\mathrm{rf0,sc0}}$	78.7	39.35
space charge parameter	Σ_{sc}	0.192	0.192
rf phase [deg]	ϕ_{rf}	0	90

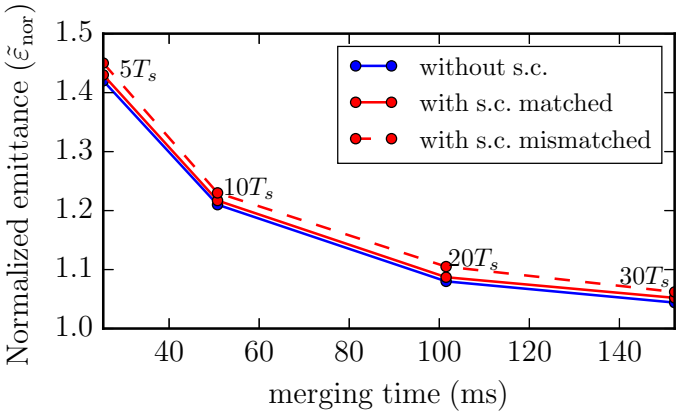

Figure 7: Comparison of the final normalized emittance with merging time of $5\mathrm{T_s}$, $10\mathrm{T_s}$, $20\mathrm{T_s}$ and $30\mathrm{T_s}$. Blue: in the absence of space charge; Red: in the presence of space charge, without (red dashed) and with (red solid) space charge matching.

but in a larger cost, and vice versa. In order to find the optimum merging time, the simulation of bunch merging in the absence of space charge under four representative merging time t_m = 5 T_{s0}, 10 T_{s0}, 20 T_{s0} and 30 T_{s0} is performed respectively by using the code pyORBIT (here 1 T_{s0} = 4.63 ms). Fig. 6 shows the simulation results of the particle distributions in the longitudinal phase-space at the beginning $t = 0$, in the middle $t = t_m/2$, and at the end $t = t_m$ in bunch merging under different merging time (For brevity only one pair of two bunches are shown, since the other is identical because of symmetry). It can be seen that the more slowly it proceeds, the better the bunches get merged, since the condition of the adiabaticity is better satisfied. Fig. 7 shows the final *normalized emittances* under different merging time. The normalized emittance is defined by

$$\tilde{\varepsilon}_{\mathrm{nor}} = \frac{\tilde{\varepsilon}_{\mathrm{sum}}}{2\tilde{\varepsilon}}. \tag{42}$$

Here, $\tilde{\varepsilon}_{\mathrm{sum}}$ is the total rms emittance of two merging bunches defined in Eq. 28, and $\tilde{\varepsilon}$ the individual rms emittance in Eq. 29. Clearly, for an ideal bunch merging, $\tilde{\varepsilon}_{\mathrm{nor}} = 1$. It can be seen from Fig. 7 that the emittance growth with merging time of 20 T_{s0} is less than that of 10%. Although the case of 30 T_{s0} has minimum emittance growth, the reduction of the emittance growth from merging time 20 T_{s0} to 30 T_{s0} is not remarkable. Taking into account the economic cost and bunch manipulation efficiency, the merging time of 20 T_{s0} (92.6 ms) is proposed for practical longitudinal manipulation in SIS100.

Secondly, in the presence of space charge the external rf voltage should be increased to com-

pensate the defocusing space charge effect. The space-charge matching voltage amplitude on the two harmonic are calculated via Eq. 38 and shown as dashed line in Fig. 5. The final normalized emittance affected by space charge with different merging time are shown as red line in Fig. 7. Compared to the case without space charge, only slight and negligible emittance growth is observed, since the defocusing space charge forces has been well-compensated via increasing the external rf voltage. In fact, the bunches can get matched to space charge during bunch merging automatically, as long as the merging proceeds sufficiently slow and the rf voltages are increased to "compensate" (get matched) to the space charge effect at the beginning and at the end of bunch merging.

5 Bunch merging affected by beam loading

5.1 Beam loading in intense hadron synchrotrons

Besides the space charge effect, another main contribution to the emittance growth during the longitudinal manipulations of high-intensity hadron beams is the effect of cavity beam loading. The beam-induced voltages (or wakefields) can be stored in the rf cavity, act on the beam itself and even on the following beams, causing a dipole oscillation and emittance growth. One of the most widely employed models of beam loading calculation is the equivalent parallel RLC resonant circuit (see, for example, Ref [19] and Ref. [20]).

In many literature, the beam loading effect is analyzed in terms of the "Phasor diagram" [12, 13], in which the beam-induced voltage and the external rf voltage are described by phasors. However, for high-intensity hadron synchrotrons with broad-band rf cavities, the higher order modes (HOM) of beam-induced voltage can not be neglected. In the following text we adopt a general expression to describe beam-induced voltages in rf cavities, which includes all the HOMs, to evaluate the effect of cavity beam loading during longitudinal beam manipulation. The beam-loading voltage V_{bl} can be solved via fast Fourier transform (FFT),

$$V_{\mathrm{bl}} = -\sum_{n=0}^{\infty} I_n Z_n e^{inz/R}, \tag{43}$$

where $I_n = q\beta c\lambda_n$ represents the n^{th}-component of beam current. In the RLC resonantor model, the n^{th}-component of cavity impedance Z_n reads

$$Z_n = \frac{R_{\mathrm{sh}}}{1 + iQ(h/n - n/h)}, \tag{44}$$

with

$$\omega = n\omega_0, \quad \omega_r = h\omega_0, \tag{45}$$

in which, R_{sh}, Q and ω_r represents the shunt impedance, the quality factor and the resonant frequency of one rf cavity, respectively; ω_0 is the revolution angular frequency.

It is worth pointing out that the current component I_n in Eq. 43 is assumed to be independent of time. In fact, the beam loading effect can be classified into the *steady-state* beam loading and the *transient* beam loading, by the decaying time (or the filling time) of the induced electric fields in the rf cavity. For a typical intense hadron synchrotron like the SIS100 discussed here, we have,

$$\omega_s \ll \frac{\omega_r}{2Q}, \tag{46}$$

which indicates the typical time-scale for synchrotron motion (described by the synchrotron frequency ω_s) is much longer than the decaying time of the induced-voltage. Therefore, we can safely neglect the "transient" beam loading effects and assume the beam current I_n in Eq. 43 is stable and independent of time.

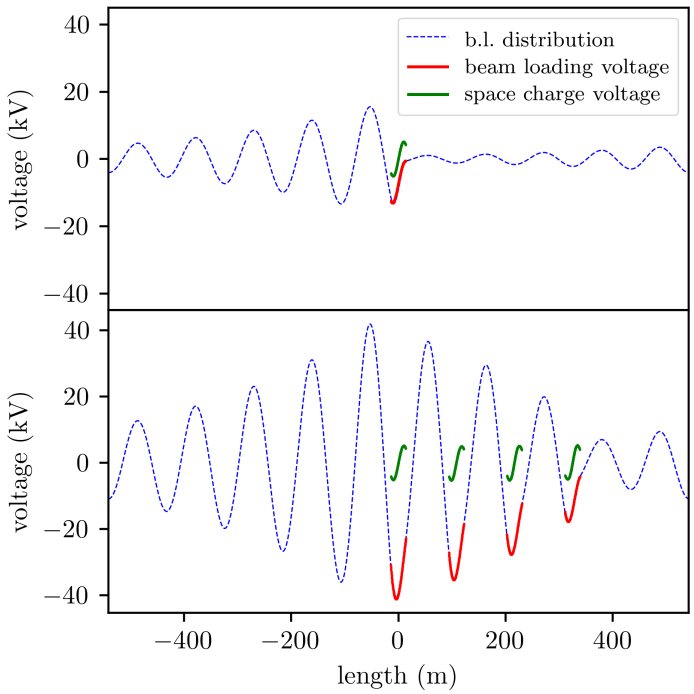

Figure 8: The beam loading voltages in seven rf cavities induced by one bunch (upper plot) and by four bunches (lower plot) in SIS-100, compared with the space charge voltages. The red and green line denotes respectively the beam-loading voltage and space charge within the beam. The dashed blue line represents the beam-loading voltage distributed along the ring.

5.2 Schemes for beam loading compensation

As discussed in Sec. 4, the longitudinal space charge is a symmetrical defocusing self-field inside the beam, and can be well "compensated" via an increased external rf voltage. In comparison, the voltage induced by the cavity beam loading effect (described as "*beam-loading voltage*" $V_{\rm bl}$ in the following text) is not symmetrical about the beam center. As an illustration, the beam-loading voltage of one bunch and four bunches induced by the seven rf cavities in SIS100 are numerically calculated via Eq. 43, and shown in Fig. 8, compared with the space charge voltages (shown as green curve in Fig. 8). One can see that for the four bunches, the amplitude of beam-loading voltages in different bunches are different: the later is larger than the former. This is because the beam-loading voltages of the former bunches can be stored in the rf cavities and can affect the following bunches.

In order to minimize the emittance growth caused by beam loading during the longitudinal manipulations, it is important to generate bunches matched to beam loading, to represent stable state of beams used for bunch merging in the simulation. Based on the two main properties of the beam loading discussed above: the asymmetry and the distance-dependence, the matched particle distribution can be obtained as follows. Firstly, the beam-loading voltage acted at the center of each bunch $V_{\rm bl0}$ is calculated using Eq. 43. Secondly, the bunches are "shifted" by $\Delta z_{\rm bl,j}$ satisfying

$$V_{\rm rf0}\sin(\Delta\phi_{\rm bl,j}) = V_{\rm bl0,j}, \tag{47}$$

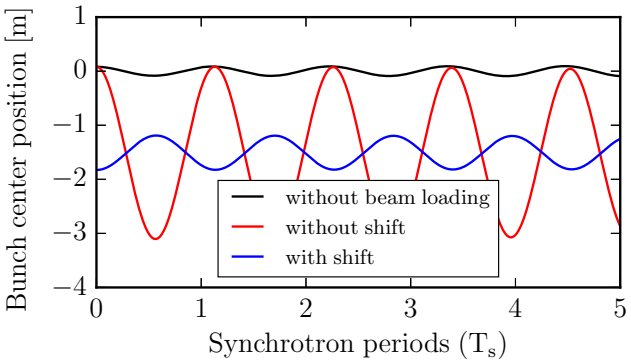

Figure 9: Evolution of beam center position with (in blue) and without (in red) the shift in Eq. 47. The red curve indicates the mismatched dipole oscillation due to beam loading, while the blue curve indicates the motion after a shift of beam center. For comparison, the case in the absence of beam loading are also shown (in black).

and

$$\frac{\Delta z_{\mathrm{bl,j}}}{\Delta \phi_{\mathrm{bl,j}}} = \frac{L}{2\pi h_i}. \tag{48}$$

Here, the subscript j is the index of the bunches for merging, and h_i is the initial harmonic number of bunch merging (for the case of SIS-100, $j = 1, 2, 3, 4$ and $h_i = h_{10} = 10$ as listed in Tab. 1). In the presence of the shifts $\Delta z_{\mathrm{bl,j}}$ on the beam centers, the external rf voltage amplitude at the center are increased to largely compensate the beam loading voltage, resulting in a much smaller amplitude of the dipole oscillation. In this sense, the bunches are matched to the beam loading effects and becomes stable.

To test the efficiency of this beam loading matching scheme of bunch center shift, Fig. 9 shows the evolution of the beam center position in five synchrotron periods (in the absence of bunch merging), with and without the bunch center shift. One can see that without the shift, the bunch behaves a visible mismatched dipole oscillation due to beam loading effect (red curve). In comparison, in the presence of a shift calculated from Eq. 47 and Eq. 48 acting on the beam center, the amplitude of the dipole oscillation is largely reduced (blue curve). The case in the absence of beam loading are also shown as black color, in which the slight oscillation is from the initial noise of the particle distribution. Therefore, the particle distribution matched to beam loading used in the simulation can be achieved via the beam-center shift scheme. Based on Eq. 47, we introduce the *beam loading parameter*, defined by the ratio of the beam loading voltage amplitude acted on the bunch center, to the external rf voltage amplitude

$$\Sigma_{\mathrm{bl}} = \frac{V_{\mathrm{bl0}}}{V_{\mathrm{rf0}}}, \tag{49}$$

to evaluate the contribution of the beam loading effect on the longitudinal beam motion. Similarly to the space charge parameter, the beam loading parameter describes the extent of the contribution of the intensity effects acting on the longitudinal beam motion.

The shifts of the beam centers introduced above can be employed for beam loading matching. However, the shifts can cause an asymmetry during bunch merging. As shown schematically in Fig. 10, the two red shaded elliptical areas represents two bunches without beam loading. The two dashed red ellipses denotes the two shifted bunches for beam loading matching. Since the beam

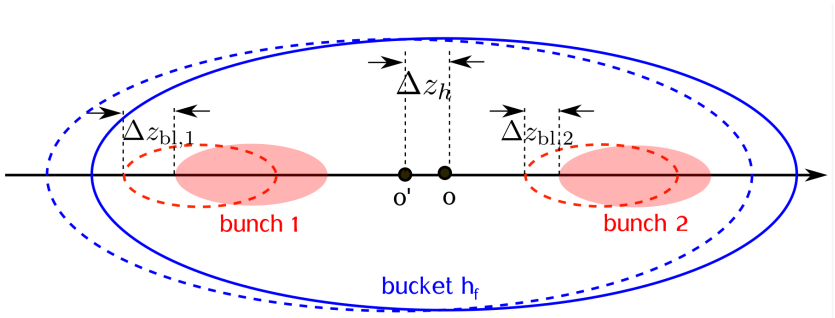

Figure 10: Schematic drawing of the beam loading matching shifts $\Delta z_{\rm bl}$, and the rf cavity shift for symmetry compensation Δz_h. The red shades and the solid blue curve denote the initial positions of the bunches without the matching shifts and the buckets in the initial harmonic h_i, respectively. The dashed red ellipses represents the bunches with beam-loading matching shifts. The dashed blue ellipse is the shifted bucket via Δz_h to keep the symmetry of the two bunches in h_f.

loading acted on the first bunch is larger than that on the second one, $V_{\rm bl0,1} > V_{\rm bl0,2}$, the matching shift of the first bunch is larger than the shift of the second, $\Delta z_{\rm bl,1} > \Delta z_{\rm bl,2}$. Consequently, with the matching shift $\Delta z_{\rm bl,2}$, the initial position of the second bunch is closer to the center of the harmonics o (the solid blue ellipse), and thus arrives earlier at the center of the harmonics during merging (The right red dashed ellipse is closer to o than the left one in Fig. 10). This "asymmetry" about the harmonic center o can bring oscillation and emittance growth during bunch merging. In order to compensate this asymmetry as much as possible, a shift $\Delta z_{\rm h}$, satisfying $\Delta z_{\rm h} = (\Delta z_{\rm bl,1} + \Delta z_{\rm bl,2})/2$, is added on the phase of the final harmonic h_f. Generally, for the bunch merging with n_b bunches, the shifts on harmonics $h^{(i)}$ becomes

$$\Delta z_{\rm h} = \frac{1}{n_b}\sum_{j=1}^{n_b} \Delta z_{\rm bl,j}. \tag{50}$$

The shift of the rf cavity $\Delta z_{\rm h}$ in Eq. 50 is not confused with the shift of the bunch $\Delta z_{\rm bl,j}$ in Eq. 47 and Eq. 48. The difference of the two types of shifts are as follows.

- *matching shift* $\Delta z_{\rm bl}$ are employed for the initial beam-loading matching;
- *symmetry shift* $\Delta z_{\rm h}$ is used for keeping the symmetry of the two moving bunches about their center during merging.

By using the two shifts, the beam loading effect can be largely reduced, as will be shown in the next section.

It should be pointed out that the schemes for beam loading matching and symmetry compensation introduced here is based on the evaluation of the beam-loading induced voltages at the beginning of bunch merging and the linear approximation of the beam-loading voltage, and thus can only partly reduce the emittance growth. In fact, as the bunches are approaching to each other during the merging process, the beam loading effect will be increasing. The larger beam loading effect on the second bunch causes a larger dipole oscillation and brings asymmetry during the merging and the symmetry of the first pair is better than the second pair, as will be shown in the simulation results in the next section.

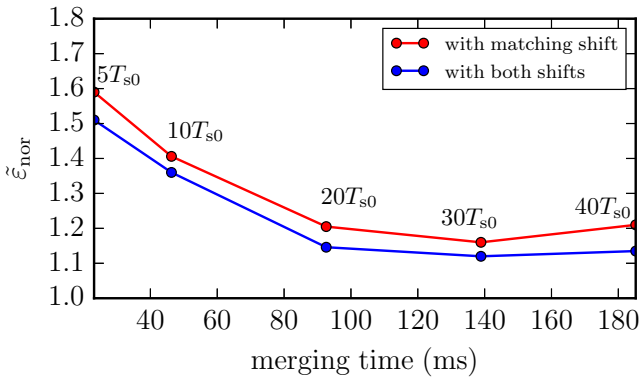

Figure 11: The normalized emittance of two bunches after bunch merging in the presence of beam loading and space charge with different merging time t_m = 5 T_{s0}, 10 T_{s0}, 20 T_{s0}, 30 T_{s0} and 40 T_{s0}: (1) with matching shift, without symmetry shifts (red); (2) with both shifts (blue).

6 Bunch merging affected by space charge and beam loading

Table 3: Beam loading parameters of the initial four proton bunches in SIS100.

Parameter [unit]	Symbol	Value
matched rf voltage with space charge [kV]	$V_{rf0,sc0}$	78.7
beam loading voltage [kV]	V_{bl0}	7.61, 9.79, 15.1, 16.2
beam loading parameter	Σ_{bl}	0.097,0.12,0.19, 0.21
matching shift [m]	Δz_{bl}	1.67, 2.15, 3.34, 3.57
shunt impedance [Ω]	R_{sh}	2000
quality factor for h_{10}	Q_{10}	10.52
quality factor for h_5	Q_5	5.26
maximum rf voltage per cavity [kV]	$V_{rf,max}$	20
total number of rf cavities	n_{cav}	14
cavity number for h_{10}	$n_{cav,h10}$	4
cavity number for h_5	$n_{cav,h5}$	2

In the preceding sections, the effect of space charge and beam loading in the bunch merging are analyzed separately. In reality, both effects have to be taken into account simultaneously. In this section bunch merging with the *combined* effect of space charge and beam loading will be investigated.

Based on the beam parameters listed in Tab. 1, the initial beam-induced voltage V_{bl0} and the corresponding matching shift Δz_{bl} are calculated via Eq. 43 and Eq. 47, with the relevant parameters listed in Tab. 3. The simulation of bunch merging in SIS100 with both of space charge and beam loading are performed. In the simulation, the matched external rf voltage amplitude in the presence of space charge ($V_{rf0,sc0}$ in Tab.2) are employed. The matching shifts (the four Δz_{bl} in Tab. 3) are added on the bunch positions for initial beam loading matching. As listed in Tab. 3, at the beginning of the bunch merging, there are four working cavities on $h_{10} = 10$ to provide the external focusing rf voltage. As the bunch merging starts, two cavities on $h_5 = 5$ are turned on.

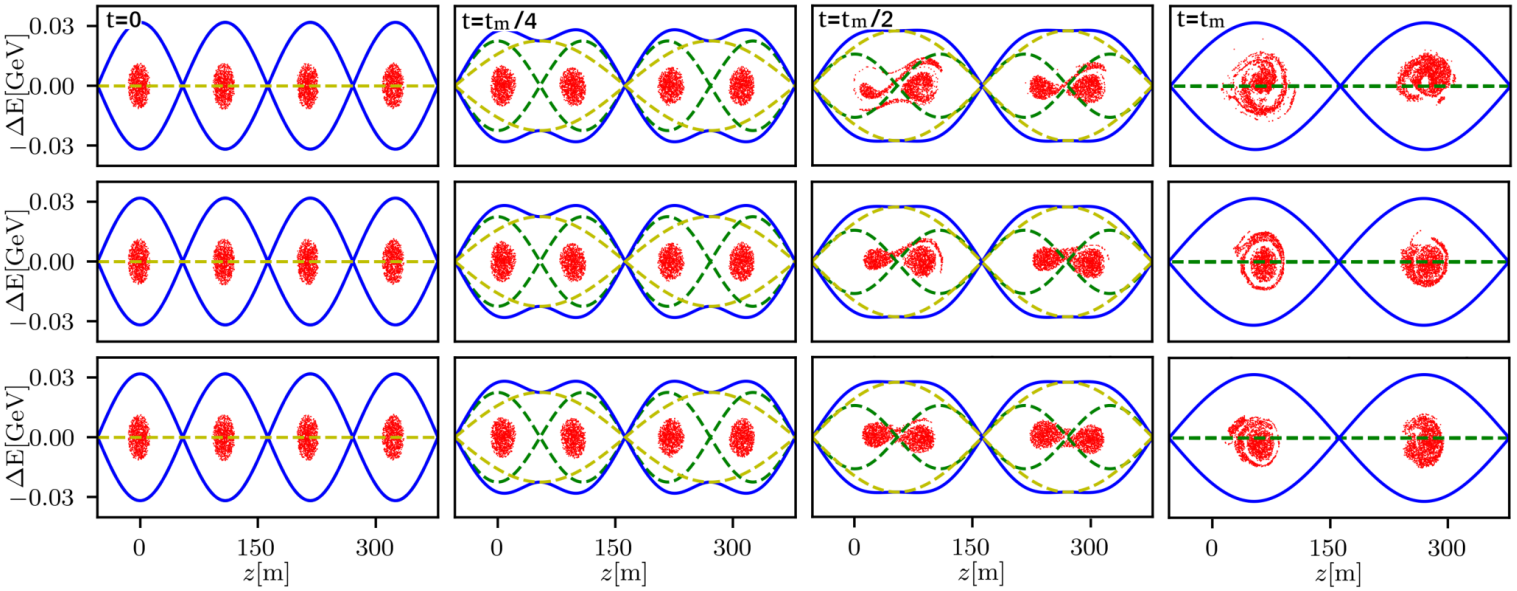

Figure 12: Particle distribution in the longitudinal phase space at the initial ($t = 0$), quarter ($t = t_{\mathrm{m}}/4$), half ($t = t_{\mathrm{m}}/2$) and end ($t = t_{\mathrm{m}}$) of bunch merging with merging time of 20 T_{s0}, in the presence of both space charge and beam loading for three cases: (upper subplot) without matching shift and symmetry shift; (middle plot) with matching, without symmetry shift; (lower subplot) with both of matching and symmetry shift. The blue curve is the separatrix orbit of the combined (dual) harmonics; the green the separatrix orbit of the harmonic $h_{10} = 10$; the yellow is the one of the harmonic $h_5 = 5$.

Therefore during bunch merging there are six rf cavities that contributes the beam loading effect.

The simulation results of the final normalized emittance after bunch merging with different merging time $t_{\rm m}$ = 5 $T_{\rm s0}$, 10 $T_{\rm s0}$, 20 $T_{\rm s0}$, 30 $T_{\rm s0}$ and 40 $T_{\rm s0}$ (the bare synchrotron period $T_{\rm s0}$ = 4.63 ms) are shown in Fig. 11. The red curve shows the bunch merging affected by space charge and beam loading with initial matching shifts $\Delta z_{\rm bl}$ on the bunch centers, but without symmetry shift Δz_h on the rf cavities ; the blue line shows the case with both of the initial matching shifts and symmetry shift. In comparison, the dashed red line denotes the case without any shifts. It can be seen that in the presence of the matching shifts and the symmetry shifts the emittance growth is dramatically dampened.

It is interesting to obverse from Fig. 11 that with longer merging time $t_{\rm m} = 40\ T_{\rm s0}$, the emittance growth becomes instead larger. Comparing the emittance growth shown in Fig. 7 and in Fig. 11, one can find that the difference on emittance growth between the case of $T_{\rm s0}$ = 20 ms and $T_{\rm s0}$ = 30 ms in Fig. 11 is smaller than that in Fig. 7. Those phenomena imply that in the presence of space charge and beam loading, a much slower bunch merging process can not achieve a better merging results because of the long acting beam loading effect. Indeed, a slower bunch merging process allows the adiabaticity condition better satisfied. However, longer merging time indicates the beam loading effect acting on the beam lasts longer, causing longer dipole oscillations. As shown in Fig. 11, in the presence of beam loading and space charge, the difference of the emittance growth between merging time 20 $T_{\rm s0}$ and 30 $T_{\rm s0}$ can be negligible. The merging time $t_{\rm m}$ = 20 ms is chosen as an optimum merging time in the presence of beam loading, and will be adopted in the following study.

Fig. 12 shows the evolution of the particle distribution during bunch merging in the presence of space charge and beam loading in SIS100 for the three cases: upper, without any shifts; middle, with initial matching shifts, but without symmetry shift; lower, with both matching shifts and symmetry shifts. In comparison between the upper and middle subplots, one can see that the bunch quality of bunch merging with an initial matching shift has much improved. Furthermore, one can observe in the middle subplot that the emittance growth of the second bunch pair is larger. This is because the beam loading on the second pair is larger. In the presence of symmetry shift (the lower subplot), the symmetry is largely compensated with smaller emittance growth.

7 Batch compression with space charge and beam loading

7.1 Phase modulation and shifts

In the proposed schemes of longitudinal manipulations of SIS100, the bunch merging is followed by the "bunch batch compression" to further compress the "bunch train". During the batch compression, the harmonic number is increasing from 5 to 10 step by step, in which the "batches" of bunched beams are handed over from the lower harmonics to the higher ones. For the manipulation of batch compression, two main points should be considered and presented as follows.

Firstly, the presence of the two rf harmonics leads to amplitude modulation of rf voltage, which affects the rf focusing and the bucket areas (longitudinal acceptance) distributed along the ring. The areas of the two tail buckets are smallest while the area of the center bucket is largest [11]. The combined sinusoidal rf voltage waveform of the two "adjacent" harmonic takes the form

$$\begin{aligned} & V_j \sin(\frac{h_j z}{R}) + V_{j+1} \sin(\frac{h_{j+1} z}{R}) \\ & = (V_j - V_{j+1}) \sin(\frac{h_j z}{R}) + 2V_{j+1} \sin(\frac{h_j + h_{j+1}}{2} \frac{z}{R}) \cos(\frac{h_j - h_{j+1}}{2} \frac{z}{R}). \end{aligned} \tag{51}$$

Here the subscript "j" denotes the harmonic number from 10 to 5, and $h_{j+1} - h_j = 1$. Eq. 51

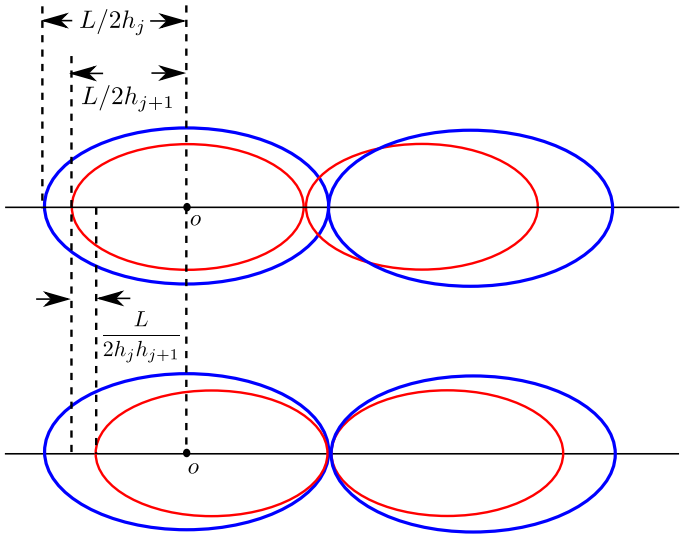

Figure 13: Schematic drawing of the relative shifts between two adjacent harmonics h_j and h_{j+1} to keep the symmetry during batch compression.

indicates that during batch compression, the modulation becomes strongest when $V_j = V_{j+1}$. Fortunately, for the batch compression of SIS100, as sketched in Fig. 1, there are only two adjacent buckets loaded with bunches. During the batch compression, the positions of the two buckets containing bunches can be chosen to be at the center of the five buckets so that the modulation effect becomes most negligible.

Secondly, during batch compression, the bunches transferred from the harmonic h_j to h_{j+1} should keep symmetry to avoid extra dipole oscillations of the bunches. The batch of the bunches should converge symmetrically towards the center of the batch. To this end, the position shift for the higher harmonic h_j ($j \geq 5$) relative to the lowest harmonic h_5 is

$$\Delta l_j = \frac{L}{2h_5} - \frac{L}{2h_j} = \frac{L(h_j - h_5)}{2h_5h_j}, \tag{52}$$

and the corresponding phase shift

$$\Delta\phi_j = \frac{2\pi h_j}{L}\Delta l_j = \frac{\pi(h_j - h_5)}{h_5}. \tag{53}$$

Fig. 13 shows schematically the relative shift between two neighbouring harmonics. For convenience, this shift for symmetry are written as *batch symmetry shift* in the following.

Furthermore, since the bunches are moving during batch compression, the rf phase for each harmonic should be shifted to synchronize with the bunches, as shown in the second term of the "rf phase"in Tab. 4. For example, at the beginning of batch compression, the center of the two bunches in harmonics $h_5 = 5$ locates at 54.18 m and 270.9 m respectively, and the corresponding rf phase is 90°. After the batch compression from $h_5 = 5$ to $h_6 = 6$, the bunches are shifted to the position at 72.24 m, which corresponds to an rf phase of 108°, and so on for other harmonics. This rf shifts for synchronize with bunch can be written as *synchronized shift* and listed in the second term of the "rf phase" in Tab. 4. In total, the rf phase shift added on the harmonics during batch compression is a summation of the two shifts, i.e.,

$$\text{rf shift} = \text{batch symmetry shift} + \text{synchronized shift}.$$

Table 4: Relevant parameters for proton bunch batch compression in SIS100.

Parameter [unit]	Symbol	Value
Initial matched rf voltage [kV]	$V_{\mathrm{rf0,sc0}}$	39.35
Initial space charge voltage [kV]	V_{sc0}	6.35
Initial harmonic	h_5	5
Final harmonic	h_{10}	10
rf phase for h_5 [deg]	ϕ_5	$0 + 90$
rf phase for h_6 [deg]	ϕ_6	$36 + 108$
rf phase for h_7 [deg]	ϕ_7	$72 + 126$
rf phase for h_8 [deg]	ϕ_8	$108 + 144$
rf phase for h_9 [deg]	ϕ_9	$144 + 162$
rf phase for h_{10} [deg]	ϕ_{10}	$180 + 180$
cavity number for h_5	$n_{\mathrm{cav,h5}}$	2
cavity number for h_6	$n_{\mathrm{cav,h6}}$	2
cavity number for h_7	$n_{\mathrm{cav,h7}}$	2
cavity number for h_8	$n_{\mathrm{cav,h8}}$	2
cavity number for h_9	$n_{\mathrm{cav,h9}}$	2
cavity number for h_{10}	$n_{\mathrm{cav,h10}}$	2

As shown in Tab. 4, the first term in "rf phase" represents the batch symmetry shifts, and the second term are the synchronized shifts.

7.2 Simulation results

Simulations of the batch compression in SIS100 are performed based on the two considerations discussed above. In the simulation, the initial two bunches are assumed to be two well-merged bunches after an ideally merging of four bunches with the example parameters in Tab. 1. The relevant settings for batch compression are listed in Tab. 4. Since the batch compression follows the bunch merging, the initial rf voltage amplitude for batch compression is equal to the final value of the matched rf voltage with space charge $V_{\mathrm{rf0,sc0}}$ in Tab. 2. The rf voltage ramps are shown in Fig. 14. The rf voltage amplitude employed in the simulation are set to be varying linearly during batch compression. For simplicity, each step of the batch compression from h_{j} to $h_{\mathrm{j+1}}$ is set to be with the same time interval $\Delta t = t_{\mathrm{j+1}} - t_{\mathrm{j}}$.

Firstly, simulations with compression time $t_{\mathrm{c}} = 100$ ms is performed. Fig. 15 shows the evolution of the particle distribution from harmonic $h_5 = 5$ to $h_{10} = 10$. The dashed and dotted lines in the figure are guides for eyes, showing the constant position of the batch center, and the change of the bunch centers during batch compression. It can be seen that with rf phase shift (i.e., the batch symmetry shift and synchronized shift in Tab. 4), the center of the two bunches keeps constant and the two bunches are covering to their center symmetrically during batch compression.

Fig. 16 shows the evolution of the particle distribution with separatrix orbit of the harmonics during the batch compression with harmonic number $h_5 = 5$ to $h_6 = 6$. One can see that how the rf system transforms from a lower harmonic to a higher one: with rf voltage amplitude decreasing in lower harmonic (h_5 in the figure) and increasing in higher harmonic (h_6 in the figure), a dual harmonic system forms ($t = 10$ ms). As external rf voltages in the two harmonics keep varying, a new bucket is "born" from the dual harmonic system ($t = 15$ ms). One can observe that the new bucket is so far away from the two buckets loaded with two bunches, that the deformation of the

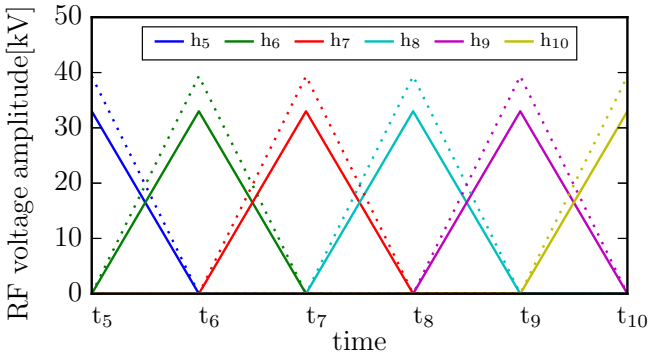

Figure 14: Proposed rf voltage ramps for proton bunch batch compression in SIS100 with (dashed line) and without (solid line) space-charge matching. Here $t_{i+1} - t_i$ denotes the batch compression time during h_i to h_{i+1}.

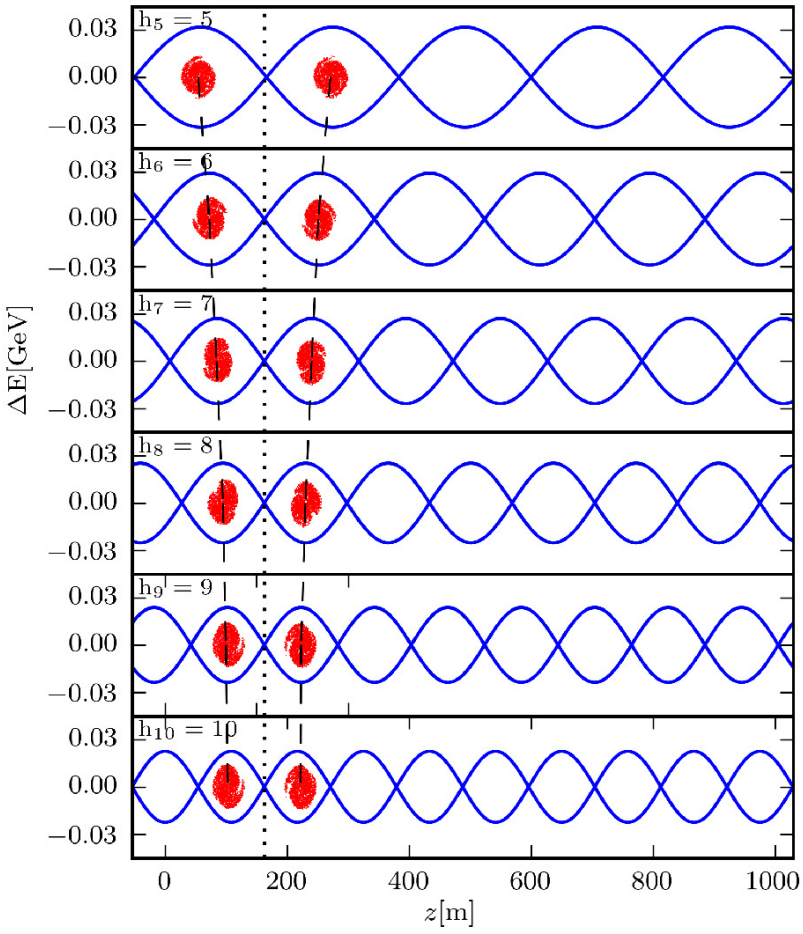

Figure 15: Snapshots of particle distribution in the longitudinal phase space during batch compression. The dashed line and dotted line serve as a guide to the eye.

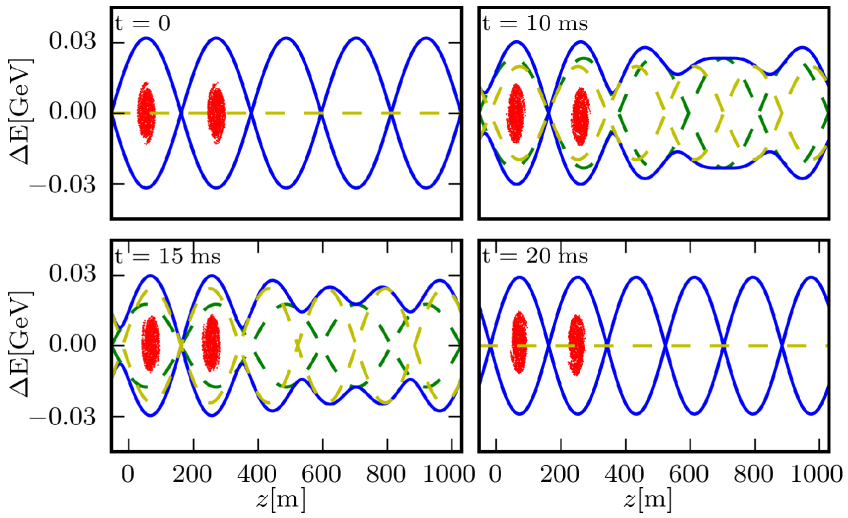

Figure 16: Particle distribution in the longitudinal phase space at the initial ($t = 0$), half ($t = 10$ ms), three quarters ($t = 15$ ms) and final ($t = 20$ ms) in the first stage ($h = 5$ to $h = 6$) of the batch compression with space charge and beam loading. The compression time from $h = 5$ to $h = 6$ is 20 ms.

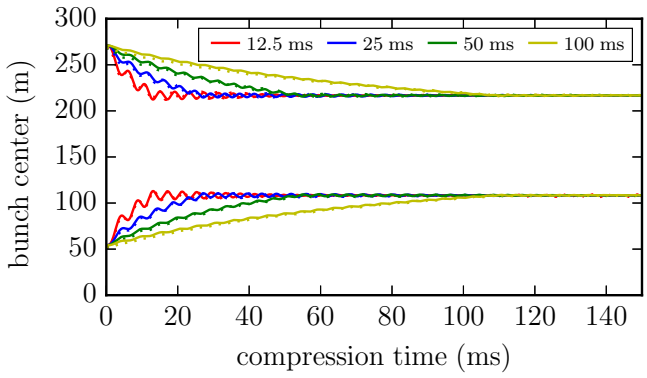

Figure 17: Evolution of the bunch centers during and after batch compression with different compression time: $t_c = 2.5T_s, 5T_s, 10T_s$ and $20T_s$, without (solid line) and with (dashed line) space charge and beam loading

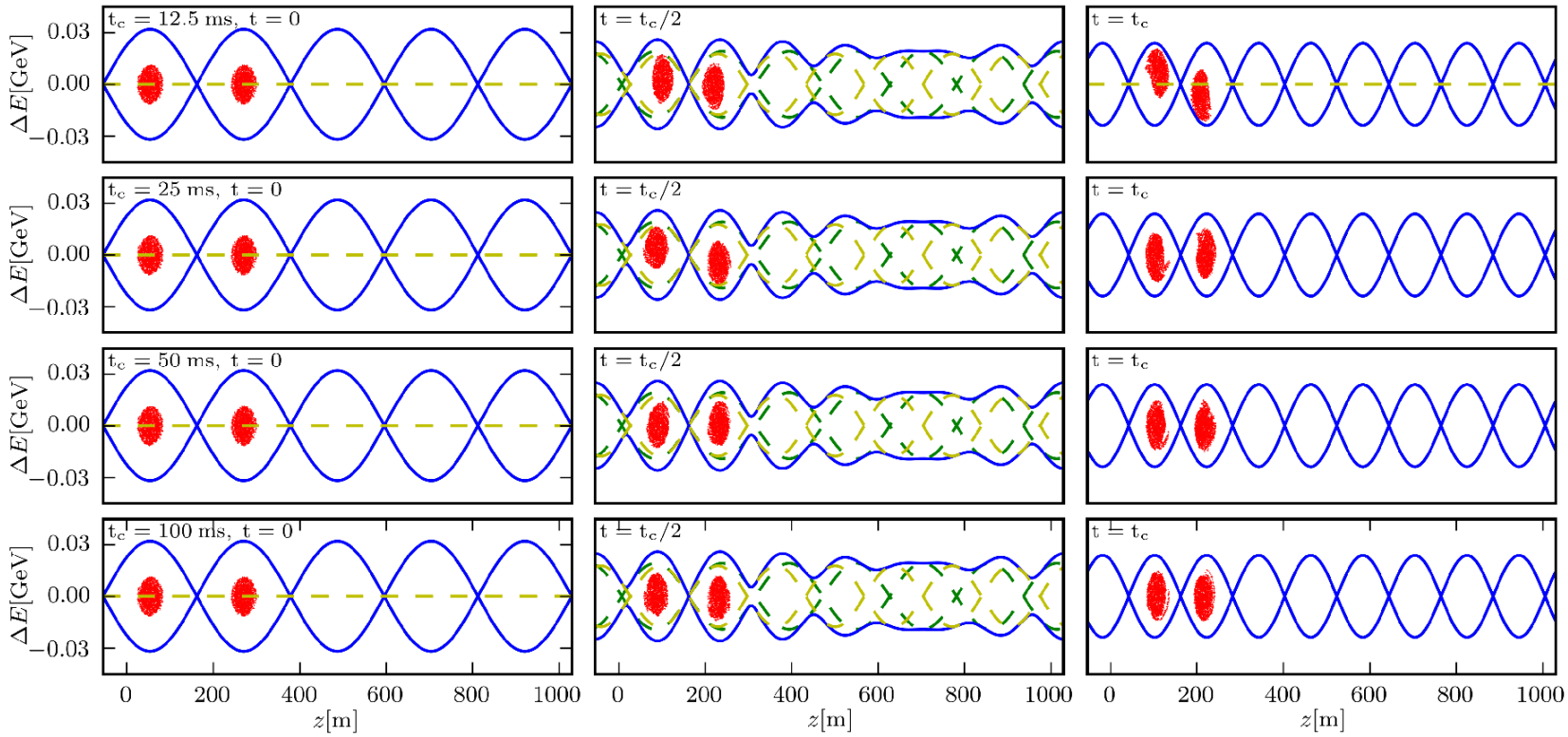

Figure 18: Particle distribution in the longitudinal phase space at the initial ($t = 0$), half ($t = 100$ms), three quarters ($t = 150$ms) and final ($t = 200$ms) of proton bunch batch compression with both of space charge and beam loading in SIS100, with compression time $t_c = 100$ms.

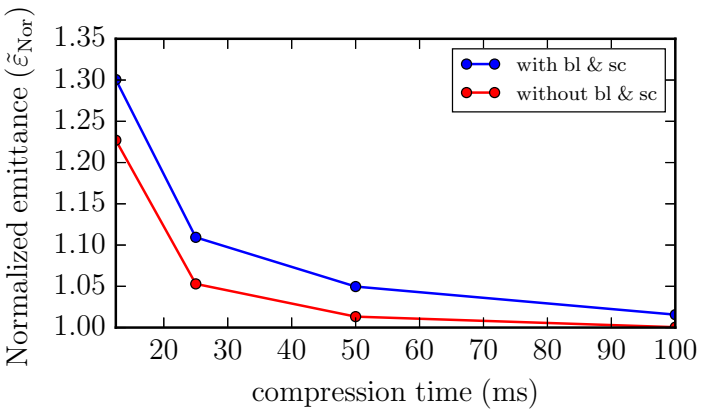

Figure 19: The average normalized final emittance of the two bunches under four different batch compression time of t_c = 12.5ms, 25ms, 50ms and 100ms for two cases: (1) in the presence of space charge and beam loading (in blue); (2) in the absence of space charge and beam loading (in red).

buckets has negligible effect on bunches (see the "voltage modulation" in Eq. 51).

Secondly, the batch compression is investigated with different compression time. Fig. 17 shows the evolution of bunch center position with four different compression time: t_c = 12.5 ms, 25 ms, 50 ms and 100 ms. Obviously, batch compression with a too short compression time (12.5 ms) can lead to a large dipole oscillation and emittance growth. Furthermore, one can observe that the dipole oscillation mainly occur within the batch compression process. Fig. 18 shows the evolution of the particle distributions during batch compression with different compression time. The dual harmonic in the intermediate time $t = t_c/2$ indicates the the largest modulation. The comparison of the three plots of the final stage of batch compression ($t = t_c$) indicate that too short compression time can lead to a large dipole oscillation and finally end up a saturated large emittance growth.

Fig. 19 shows the average final normalized emittance of the two bunches under different compression time with and without space charge and beam loading effects. With sufficiently long batch compression time (t_c = 100 ms), the space charge and beam loading has only a few percent contribution ($< 3\%$) to the emittance growth is observed, this is contributed by both the dipole oscillation and intensity effects. In the absence of space charge and beam loading, the small emittance growth is due to the dipole oscillation.

In the simulation of batch compression presented above, we have taken into account the space charge compensation voltage, but didn't adopt any schemes for beam-loading compensation. As shown in Fig. 19, with a sufficiently long compression time (i.e., $t_c \geq 50$ ms), the emittance growth due to space charge and beam loading is less than 5%, which is much lower than the case in bunch merging (see Fig. 7 and Fig. 11). In fact, during batch compression the two bunches are handed over by harmonics with positions shifted. In comparison, during the bunch merging, the two bunches are approaching to each other and finally get merged. Compared to the effects of beam loading and space charge in bunch merging in Fig 12, the contribution from space charge and beam loading to emittance growth during batch compression is much less. Therefore, during batch compression the beam loading effect is tolerable without any beam loading compensation schemes.

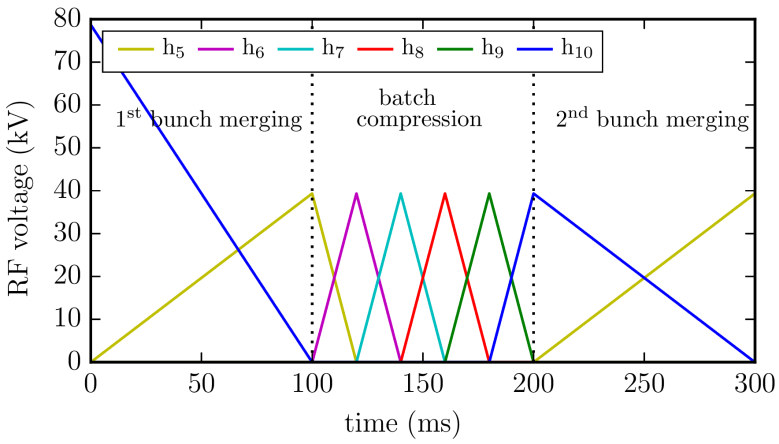

Figure 20: Proposed rf voltage amplitude ramps for the full longitudinal manipulation of proton bunches.

8 Complete RF manipulation scheme for proton bunches

Based on the above analysis of bunch merging and batch compression, now we get ready to perform the simulation of the full longitudinal manipulations of proton bunches in SIS100, which includes three parts: a first bunch merging, a batch compression and a second bunch merging, as shown in Fig. 1. There are several considerations of the settings for the full longitudinal manipulation. First of all, it is important to choose an appropriate compression time periods. As discussed in Sec. 6, on the one hand, a minimum longitudinal emittance growth requires a sufficiently long compression time period. On the other hand, the longitudinal manipulations of the bunches should be done as fast as possible to avoid long term intensity effects and minimize the costs of the accelerator operation. Secondly, the external applied rf voltage and rf phases should be set correctly via the schemes proposed in Sec. 5, to achieve a symmetrical bunch compression and compensate the intensity effects, especially for bunch merging. Finally, the external rf voltage should be practically in the range that the rf cavity can offer: for the 14 rf cavities of SIS100, the total available rf voltage amplitude is 280 kV (a maximum of 20 kV for each cavity).

8.1 RF voltages and phases

Taking all the above aspects into account, main longitudinal parameters and settings are proposed and presented in Tab.5. Based on the schemes presented in the foregoing sections, the layout of the external rf voltage amplitude ramps are shown in Fig. 20. The initial rf voltages are matched to space charge. The compression time in each stage is chosen to be 100 ms, which is sufficiently long for a low emittance growth (see Fig. 11 and Fig. 19).

The design of the external rf voltage amplitude for each stage are introduced as follows. Firstly, for the first bunch merging, the rf voltage amplitude on harmonic h_{10} and h_5 are designed in such a way so as to keep a constant bunching factor and match to space charge effect, (Eq. 40 and Eq. 41). The initial matched voltage amplitude is 78.7 kV, which requires 4 rf cavities on working. The rf phase on harmonic h_{10} are set to be zero, and the rf phase on harmonic h_5 is 94.5°, which includes two parts: the 90° for the relative phase between h_{10} and h_5 (see Fig. 2), and the 4.5° for beam loading symmetry shift (see Eq. 50). The initial bunch positions are set to match the initial beam loading effect (see Eq. 47). Secondly, for the batch compression, the maximum rf voltage amplitudes on each harmonic from h_5 to h_{10} are set to be the same value, which is equal to the

Table 5: Main parameters for the proton bunch longitudinal manipulation in SIS100 in the first example

Parameter [unit]	Initial	1^{st} Bunch merging	Batch compression	2^{nd} Bunch merging
rf voltage amplitude [kV]	78.7	39.35	39.35	39.35
harmonic number	10	5	10	5
bare synchrotron tune [$\times 10^{-4}$]	8.0	4.0	5.6	4.0
compression time [ms]	-	100	100	100
h_{10} phase [deg]	0	0	180 + 180	270
h_9 phase [deg]	-	-	144 + 162	-
h_8 phase [deg]	-	-	108 + 144	-
h_7 phase [deg]	-	-	72 + 126	-
h_6 phase [deg]	-	-	36 + 108	-
h_5 phase [deg]	90 + 4.5	0	0 + 90	90
rms bunch lengths [m]	6.25, 6.25, 6.25, 6.25	13.4, 14.1	12.1, 13.9	23.5
rms momentum spreads [$\times 10^{-3}$]	1.11, 1.11, 1.11, 1.11	1.31, 1.42	1.52, 1.58	1.89
bunch positions[m]	-3.35, 105.2, 214.6, 323.4	52.7, 272.1	109.1, 216.4	162.7
cavity numbers	6	6	4	4

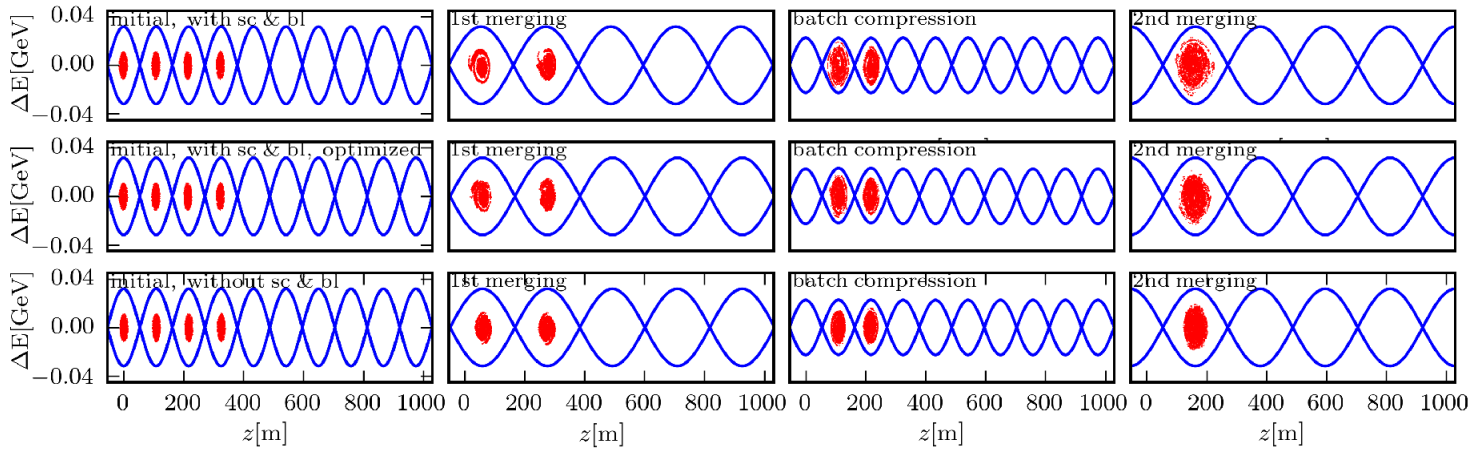

Figure 21: Particle distribution in the longitudinal phase space during proton bunches manipulations in SIS100 at the initial, end of first bunch merging, end of batch compression and the end of second merging in the presence of both of space charge and beam loading for three cases: upper plot: with initial matching shift, without symmetry shifts; middle plot: with both of initial matching shifts and symmetry shifts; lower plot: ideal case. i.e., without space charge and beam loading.

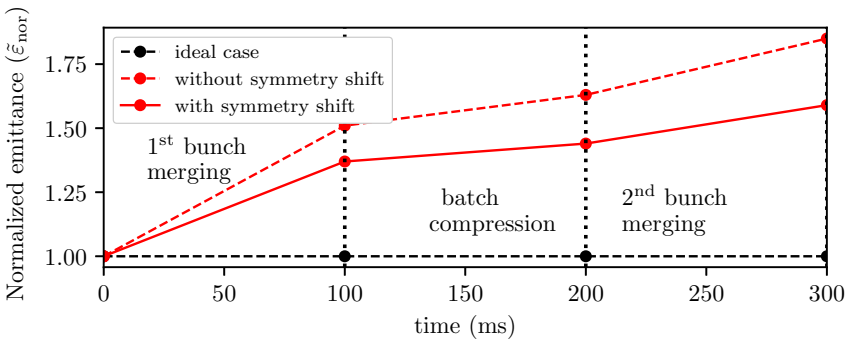

Figure 22: The normalized longitudinal emittance at each stage of the proton bunch longitudinal manipulation for three cases: the ideal case (black); the case affected by intensity, without symmetry shift (red); the case affected by intensity, with symmetry shift (blue).

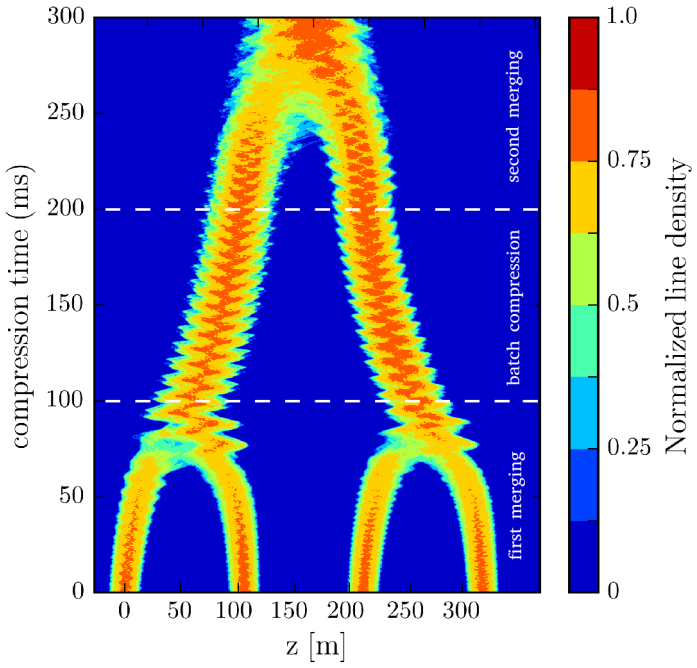

Figure 23: The "waterfall" plot of the bunch density during the proton bunch longitudinal manipulation.

Table 6: Emittance growth, bunching factor and transverse tune shifts (horizontal and vertical) during proton bunch manipulation in FAIR SIS100

Parameter [unit]	Initial	1^{st} Bunch merging	Batch compression	2^{nd} Bunch merging
emittance growth	-	36%	44%	59%
bunching factor	0.26	0.28	0.53	0.48
horizontal tune shift	0.07	0.07	0.09	0.11
vertical tune shift	0.12	0.12	0.14	0.18

final value of the bunch merging (39.35 kV). The rf phase for each harmonic consists of two parts: the symmetry shift and the synchronized shift, which adopts the same configuration as presented in Sec. 7 (see Tab. 4). Thirdly, for the second bunch merging, the rf phase on h_{10} is set to be 270° to match the shifted bunch positions. In order to achieve a bunch merging with constant bunching factor, the required rf voltage amplitudes on the final harmonics $h_{10} = 10$ should be 19.68 kV (half of the 39.35 kV). However, simulation shows that the emittance growth contributed by beam loading of two rf cavities is slight and acceptable. Therefore, we keep the same voltage amplitude 39.35 kV for the last bunch merging to obtain a higher beam intensity in the final bunch.

8.2 First example of the proton bunch manipulation

1" Based on the above proposed parameters and settings, an simulation example of the full longitudinal manipulation of proton bunches in FAIR SIS100 are performed. The simulation results of the particle distribution with and without intensity effects are shown in Fig. 21. During the first bunch merging, four bunches in two pairs on harmonic h_{10} are firstly merged into one bunch pair on h_5. Due to the stronger beam loading effect, the emittance growth of the second bunch is larger than the emittance of the first bunch. The first merging is followed by the batch compression, during which the two bunches are compressed with harmonics varying from h_5 to h_{10}. Finally, a second bunch merging proceeds from h_{10} to h_5, in which the two bunches get merged into one bunch. The longitudinal manipulation with intensity effect (upper and middle plot) has a larger emittance than the ideal manipulation (lower plot). Furthermore, compared to the the upper plot, the smaller emittance growth in the middle plot indicates that the emittance growth due to the high intensity effects can be partly dampened via the initial beam loading symmetry shift.

Fig. 22 shows the normalized longitudinal emittances at each stage during the longitudinal manipulation affected by beam loading and space charge (the red solid line in the figure), compared with the ideal case (the blue line in the figure). The normalized longitudinal emittance per bunch is equal to one (unit) at the beginning of the bunch merging, and will be ideally doubled when the two bunches get merged after the first merging. In comparison, the emittance growth caused by intensity effects (beam loading and space charge) can be observed (shown in red dashed line). In the presence of the beam-loading symmetry shifts, the longitudinal emittance growth can be partly dampened (red solid line). During the batch compression, slight emittance growth can be observed due to intensity effects. During the final bunch merging, the two bunches are merged into one bunch, the emittance will be doubled from 2 to 4 for the ideal case. For the full manipulation, 43% emittance growth affected by intensity effects can be observed in the presence of intensity effects.

Tab. 6 lists the emittance growth and the transverse tune shift (see Appendix II) of each stage of the longitudinal manipulation. One can see that the transverse tune shifts $\Delta\nu_x$ keep constant for a constant bunching factor. The largest transverse tune shift is less than 10%, which is tolerable

for the transverse beam dynamics design of FAIR SIS100. A "waterfall" plot of the evolution of the line density during the proton bunch manipulation are shown in Fig. 23. It can be observed that the four initial bunches, with the line density increasing and oscillating during the manipulation, develops into a final compressed bunch.

8.3 Second example of the proton bunch manipulation

Table 7: Relevant initial parameters for the proton bunches in the second example.

Parameter [unit]	Symbol	Value
bare synchrotron tune	Q_{s0}	1.38×10^{-3}
rms bunch length [m]	$\tilde{z}_m$	4.43
rms momentum spread	$\tilde{\delta}_m$	2.3×10^{-3}
RF voltage on h_{10} [kV]	V_{rf0}	66.0
matched RF voltage on h_{10} [kV]	$V_{rf0,sc0}$	104.3
space charge voltage [kV]	V_{sc0}	38.3
beam loading voltages [kV]	V_{bl0}	26.5, 24.2 , 17.2, 13.9
beam loading shifts [m]	Δz_{bl}	2.89, 2.55, 1.69, 1.31
space charge parameter	Σ_{sc}	0.58
beam loading parameters	Σ_{bl}	0.254, 0.232, 0.165, 0.133
rf phase on h_5 [deg]	ϕ_5	0
rf phase on h_{10} [deg]	ϕ_{10}	90
cavity number for h_{10}	$n_{cav,h10}$	5
cavity number for h_5	$n_{cav,h5}$	3
Shunt impedance [Ω]	R_{sh}	2000

As another example of proton bunch manipulation, here we perform the simulation with an initial emittance that is half of the value listed in Tab. 1, with the bunch length and bunch height scaling down by $\sqrt{2}$, as shown in Tab. 7. Compared to the parameters in Tab. 1, it can be seen in Tab. 7 that the space charge parameter and the beam loading parameter become larger, since the bunch length is shortened and the bunch density enhanced with the halved emittance. The simulation results of the evolution of the particle distribution are shown in Fig. 25. The comparison of the (normalized) emittance growth of the two examples are shown in Fig. 26. It can be seen that although the emittance growth ratio of the second example is larger than that of the first example, the normalized emittance growth in the second example is smaller. Therefore, the parameters of the second example is proposed for the proton bunch longitudinal manipulation in FAIR SIS100.

8.4 Proton manipulation with beam loading effects contributed from total rf cavities

The simulation results in the previous subsections show the results of the proton bunch manipulation in the presence of the beam loading from the activated rf cavities. In the following, we will investigate a more realistic case, in which the proton bunch manipulation is affected by the beam loading from all the 14 rf cavities, including both the activated cavities and the inactivated cavities. In order to minimize the contributed from the inactivated cavities, the resonant frequency for inactivated cavities is chosen to be $h = 8$ (or *parking frequency*), which is far away from both

Table 8: Proposed parameters for the proton bunch longitudinal manipulation in the second example

Parameter [unit]	Initial value	1^{st} Bunch merging	1^{st} batch compression	2^{nd} bunch merging
2^{nd} compression				
rf voltage amplitude [kV]	104.3	52.2	52.2	26.1
harmonic number	10	5	10	5
bare synchrotron tune [$\times 10^{-4}$]	8.0	4.0	5.6	4.0
compression time [ms]	-	100	100	100
h_{10} phase [deg]	0	0	180 + 180	0
h_9 phase [deg]	-	-	144 + 162	-
h_8 phase [deg]	-	-	108 + 144	-
h_7 phase [deg]	-	-	72 + 126	-
h_6 phase [deg]	-	-	36 + 108	-
h_5 phase [deg]	90 + 4.5	0	0 + 90	90
rms bunch lengths [m]	4.42, 4.42, 4.42, 4.42	11.3, 10.7	11.7, 11.5	23.7
rms momentum spreads [$\times 10^{-3}$]	0.785 , 0.785 , 0.785 , 0.785	0.821, 0.851	1.11, 1.17	1.32
bunch positions[m]	-2.84, 105.8, 215.1, 323.8	51.5, 270.2	107.7, 214.9	161.2
cavity numbers	8	8	6	6

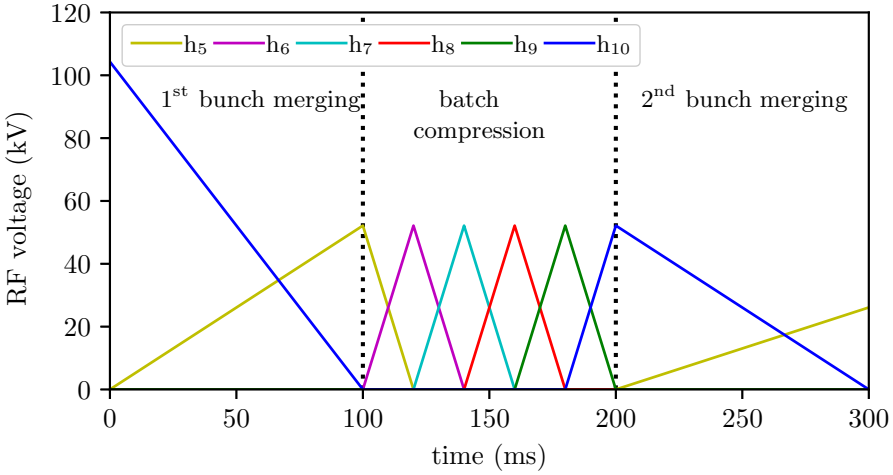

Figure 24: Proposed proton bunch compression schemes in the second example

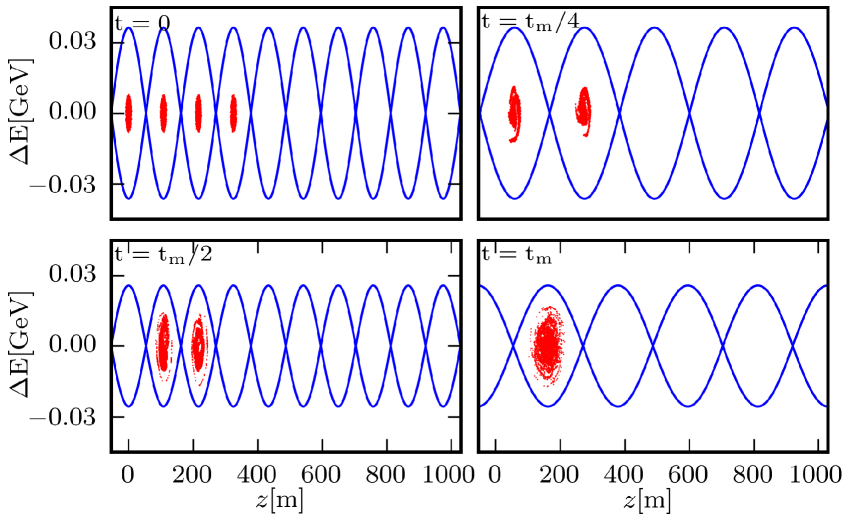

Figure 25: Particle distribution in the longitudinal phase space during proton bunch manipulation in the second example, in the presence of space charge and beam loading

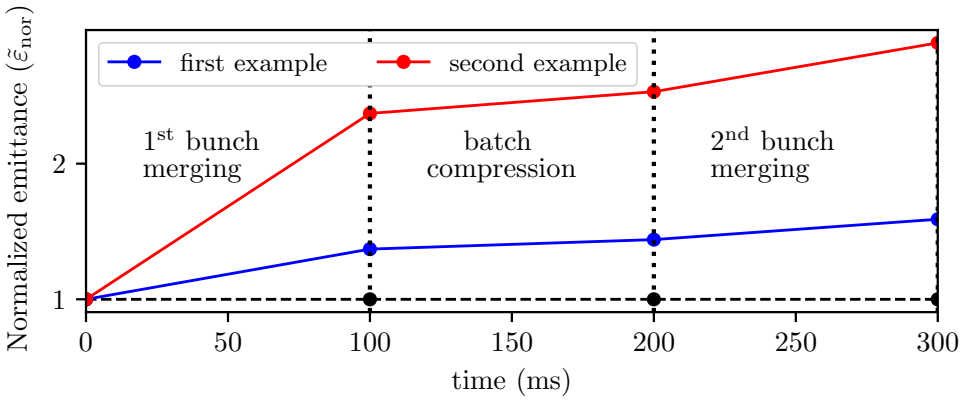

Figure 26: Comparison of the normalized longitudinal emittance at the end of each stage of the proton bunch manipulation for the first example (blue) and the second example (red). The dashed lines show the ideal cases; the solid lines show the case affected by intensity effects.

the initial harmonic $h = 10$ and the final harmonic $h = 5$ (as plotted in Fig. 27), and thus can bring the minimum additional emittance growth.

The simulation results of the emittance growth during proton bunch manipulation in the presence of total rf cavities are shown in Fig. 28. Compared to the emittance growth affected by the activated rf cavities (shown as blue line), the beam loading of inactivated rf cavities brings some moderate additional emittance growth.

Table 9: Comparison of the parameters between the activated cavities and the inactivated cavities.

	Harmonic	Q-value	Shunt impedance [kΩ]
Initial	10	10.52	2.0
Final	5	5.26	2.0
Parking	8	8.42	2.0

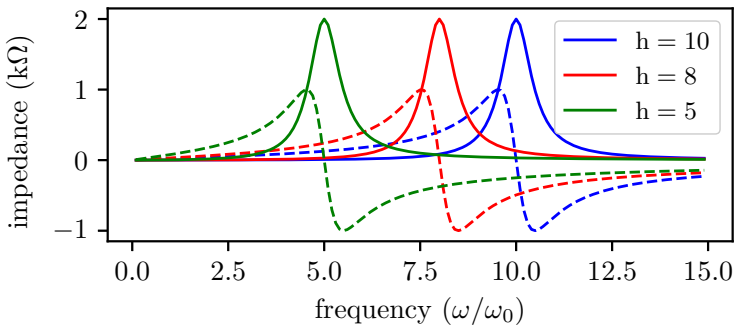

Figure 27: The cavity impedance in different resonant frequencies.

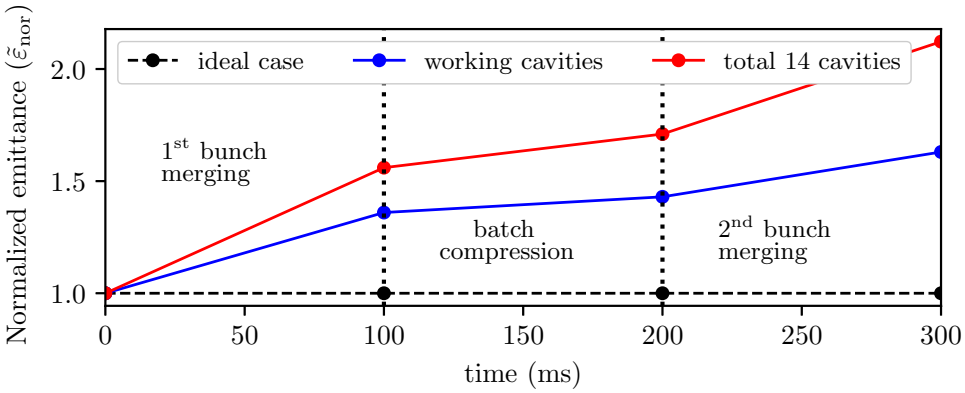

Figure 28: Comparison of the emittance growth during proton bunch manipulation affected by the beam loading of the activated rf cavities and the beam loading of the total rf cavities. The inactivated cavities are "parked" at h = 8

9 Heavy ion bunch manipulations with fast bunch rotation

In this section we investigate the longitudinal manipulation of heavy ion (U^{28+}) bunch in FAIR SIS100. In order to achieve a short intense bunch, a fast bunch rotation will be performed, besides the bunch merging and batch compression. As shown schematically in Fig. 29, it consists of a sequence of five compression stages: the first bunch merging, the first batch compression (from $h = 5$ to $h = 10$), the second bunch merging, a second batch compression (from $h = 5$ to $h = 6$), and a fast rotation of the two bunches. Here the two-bunch rotation scheme is adopted to shorten the compression time.

9.1 Heavy ion bunch manipulation with a two-bunch rotation scheme

Main beam parameters and settings of the initial intensity effects are listed in Tab. 10. The corresponding external rf voltage amplitude are proposed and shown in Fig. 30. The initial voltage amplitude is matched to space charge. For the first merging and first batch compression, the voltage amplitude in $h = 5$ increases fast to ensure a sufficient bucket area (acceptance area) to hold the bunch. For the second bunch merging, the halved voltage amplitude on $h = 5$ is employed to generate a longer bunch length, to prepare for the generation of a short bunch length during the fast bunch rotation. Finally, two bunches are rotated by a 90° in the longitudinal phase space simultaneously. The whole longitudinal manipulation of the heavy ion beam lasts for 120 ms. Main parameters of the beam loading model for the bunch compression cavities are listed in Tab. 11.

Table 10: Main parameters and initial intensity effects settings for the scenario of U^{28+} bunch longitudinal manipulation in FAIR SIS100.

Parameter [unit]	Symbol	Value
Atomic mass	A	238.0
Charge state	Z	28.0
Kinetic energy [GeV/u]	E_k	1.5
Intensity per bunch	N	6.25×10^{10}
Slip factor	η	-0.144
Initial bare synchrotron tune	Q_{s0}	1.38×10^{-3}
Initial rms bunch length [m]	$\tilde{z}_m$	11.6
Initial rms momentum spread	$\tilde{\delta}_m$	1.1×10^{-4}
matched rf voltage [kV]	$V_{\mathrm{rf0,sc0}}$	8.1
space charge voltage [kV]	V_{sc0}	3.7
beam loading shifts [m]	Δz_{bl}	4.6, 4.7, 4.8, 4.8
		5.2, 5.1, 5.3, 5.2
space charge parameter	Σ_{sc}	0.84
beam loading parameter	Σ_{bl}	0.29
RF phase on h_{10} [deg]	ϕ_{10}	0
RF phase on h_5 [deg]	ϕ_5	$90 + 8.3$

Based on the proposed settings above, the simulation of the heavy ion manipulation is performed with the voltage ramp scheme and the intensity-effect settings. In the simulation, the initial bunch positions are shifted for beam loading matching, as shown in Tab. 10. The simulation results are shown in Fig. 31, in which the particle distribution and the separatrix orbit of the bucket are represented by the red points and the blue curves, respectively. It can be seen that for the first

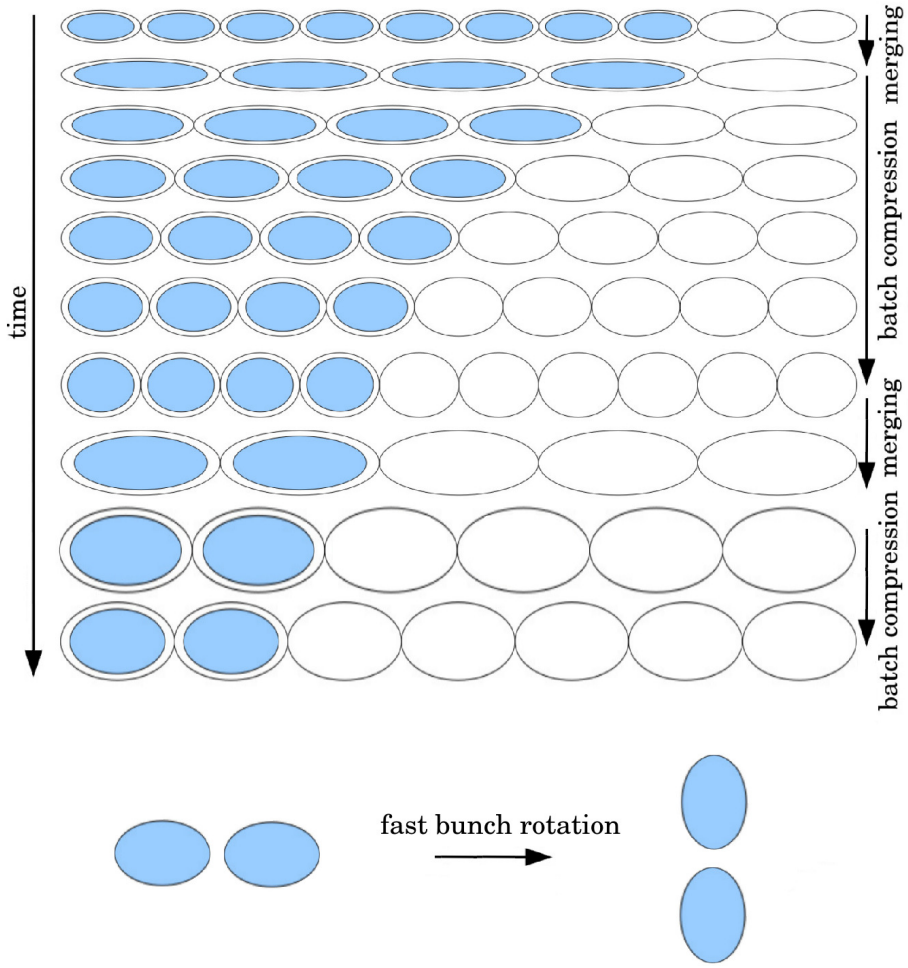

Figure 29: Proposed longitudinal manipulation scheme for heavy ion (U^{238+}) bunch compression in the future FAIR SIS100. Upper plot: the sequence of bunch merging and batch compression; Lower plot: Fast bunch rotation.

Table 11: Beam loading parameters for the bunch compressor rf cavities

Parameter [unit]	Symbol	Value
quality factor	Q	2
shunt impedance [Ω]	$R_{\rm sh}$	1000
harmonic number	h	2
number of cavities	$n_{\rm cav}$	9
maximum voltage per cavity [kV]	$V_{\rm rf}$	40
voltage for rotation [kV]	$V_{\rm rot}$	360

Table 12: Target and final parameters of the heavy ion bunch after fast bunch rotation (the parameter σ is the rms value)

Parameter [unit]	Symbol	Value
particle percentage within 70 ns window	ξ	81%
(2σ) bunch length [ns] (target/final)	τ_f	70 / 84
(2σ) momentum spread (target/final)	$\Delta p/p_f$	5×10^{-3} / 4.79×10^{-3}

bunch merging, there are "gaps" in the merged bunches, since it is a fast merging process (30 ms). For the first batch compression, the voltage amplitudes from $h = 5$ to $h = 10$ is set to be increasing to provide sufficiently large longitudinal acceptance (bucket area). For the second merging stage, the merging time is chosen to be 20 ms, since the two bunches are closer and thus they are much easier to get merged.

In order to find an optimum bunch rotation scheme, bunch rotation at $h = 5$ and $h = 6$, as well as its intermediate stage "$h = 5.5$" are compared. Here we introduce the particle percentage within the target bunch length of 70 ns, to evaluate the efficiency of the bunch rotation. The target bunch parameters for are listed in Tab. 14. Simulation results of particle percentages are shown in Fig. 32. The vertical axis represents the particle percentage in 70 ns time window of the target bunch length. It can be seen that in the presence of beam loading and space charge (solid line), the particle percentage has its maximum at $h = 6$. A longer bunch distance ($h = 5$) causes a larger filamentation; and a shorter bunch distance leads to a larger beam loading effect. Fig. 33 shows the comparison of the two bunches after the 90° rotation in the final stage with and without intensity effects. It can be seen that the filamentation exists due to the momentum spared, and evolve into two long "tails" of the bunches, causing a low particle percentage. In comparison, it is interesting to see that in the presence of intensity effect, the filamentation phenomena is largely dampened. We attribute it to the beam loading damping effect on the filamentation, which needs a further study.

9.2 Heavy ion bunch manipulation with beam loading from the total rf cavities

In this subsection we investigate the heavy ion longitudinal manipulation affected by the beam loading effects contributed by the total 14 rf cavities, as well as the 9 compressor cavities. The inactivated rf cavities are parked at harmonic $h = 8$ to minimize the beam loading effect. The emittance growth during the longitudinal manipulation are shown in Fig. 34. It can be seen that in the presence of the total 14 rf cavities , only slight emittance growth are observed. This is because the inactivated cavities are parked at $h = 8$, which is far away from the initial $h = 10$ and the final

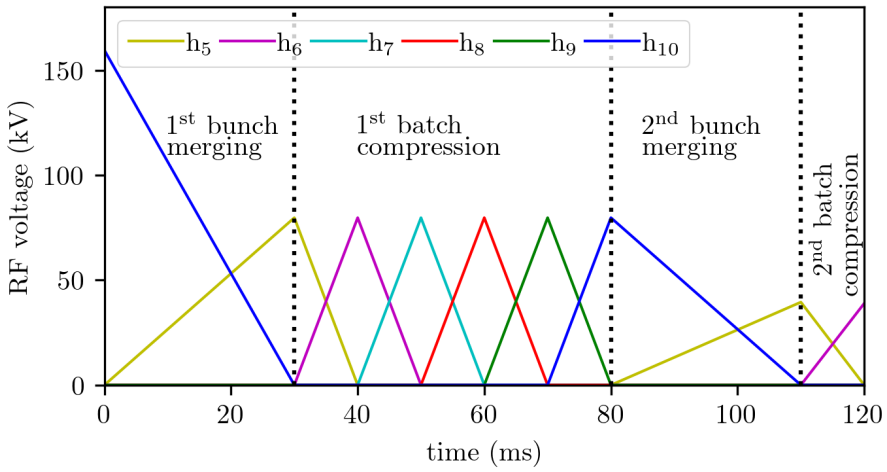

Figure 30: The rf voltage amplitude ramps during bunch merging and batch compression for the heavy ion (U^{28+}) manipulation.

harmonic $h = 5$, thus only contributes small additional impedance. The dashed blue line in Fig. 34 denotes the zero intensity case, in which space charge and beam loading are absent. The emittance growth is mainly contributed by the fast bunch merging. The dashed red line in Fig. 34 indicates the "worst case", which takes into account the beam loading from all of the rf cavities, including the 14 rf cavities for bunch merging and batch compression, as well as the 9 compressor cavities for the fast bunch rotation. Different from the 14 regular rf cavities, those 9 compressor cavities are always sitting on the harmonic h = 2. For a comparison, the case with beam loading from the activated rf cavities and the compressor cavities (see dotted line in Fig. 34) are also plotted.

The final particle percentage within 70 ns time window as well as the final bunch length are listed in Tab.14. The 6 columns corresponds respectively to the 6 cases shown in Fig.34.

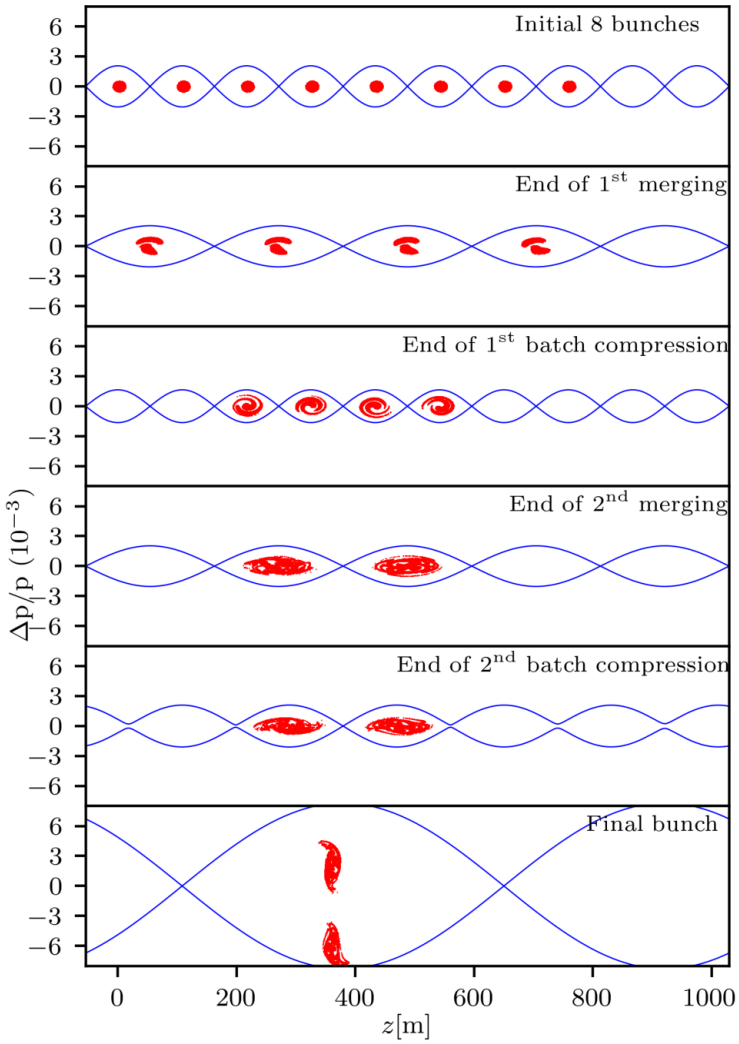

Figure 31: Particle distribution in the longitudinal phase space during longitudinal manipulation of U^{28+} bunch, in the presence of space charge and beam loading. The blue orbit and the red points represents the bucket and the particle distribution.

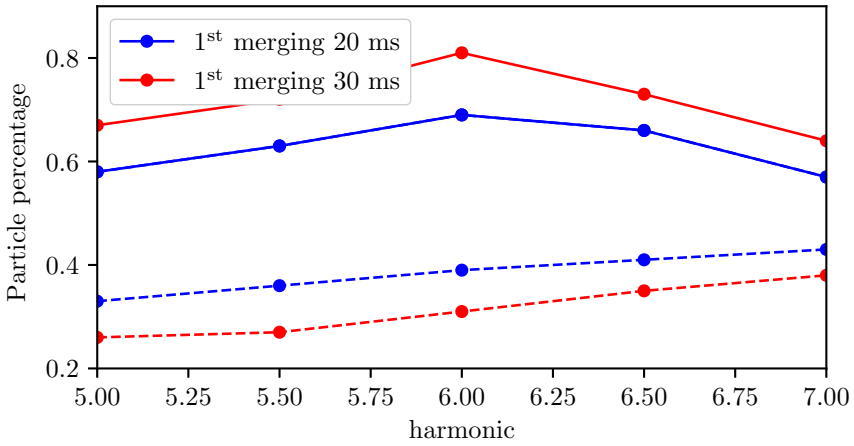

Figure 32: Particle percentage within 70 ns window in the final compressed bunch. Comparison for the fast bunch rotation with different bunch distance, in the presence of (solid line) and in the absence of (dashed line) beam loading and space charge. Red: two bunches merged from 30 ms first merging; Blue: two bunches merged from 20 ms first merging.

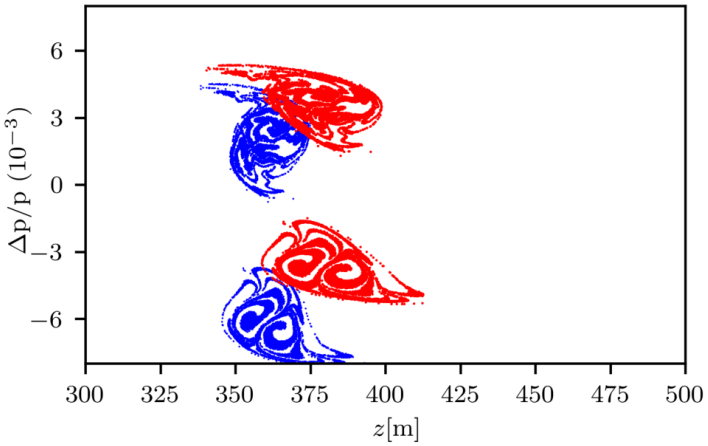

Figure 33: Comparison of the final bunch fast rotation in the presence (blue) and in the absence (red) of intensity effects.

Table 13: Proposed parameters for the heavy ion (U^{28+}) bunch longitudinal manipulation in FAIR SIS100

Parameter [unit]	Initial	1^{st} merging	1^{st} compression	2^{nd} merging	2^{nd} compression	Fast rotation
rf voltage [kV]	159.5	79.7	79.7	39.5	38.9	360.0
harmonic number	10	5	10	5	6	2
duration time [ms]	-	30	50	30	10	1.2
h_{10} phase [deg]	0	0	$180 \times 3 + 180$	0	$180 \times 3 + 180$	0
h_9 phase [deg]	-	-	$144 \times 3 + 162$	-	$144 \times 3 + 162$	0
h_8 phase [deg]	-	-	$108 \times 3 + 144$	-	$108 \times 3 + 144$	0
h_7 phase [deg]	-	-	$72 \times 3 + 126$	-	$72 \times 3 + 126$	0
h_6 phase [deg]	-	-	$36 \times 3 + 108$	-	$36 \times 3 + 108$	0
h_5 phase [deg]	$90 + 4.3$	0	$0 + 90$	90	270	0
h_2 phase [deg]	0	0	0	0	0	252
cavity numbers	12	8	8	8	6	9
rms bunch length [m]	5.0	11.2	11.6	26.1	23.6	11.5
rms momentum spread ($\times 10^{-4}$)	2.5	5.1	4.9	4.7	5.5	21.7

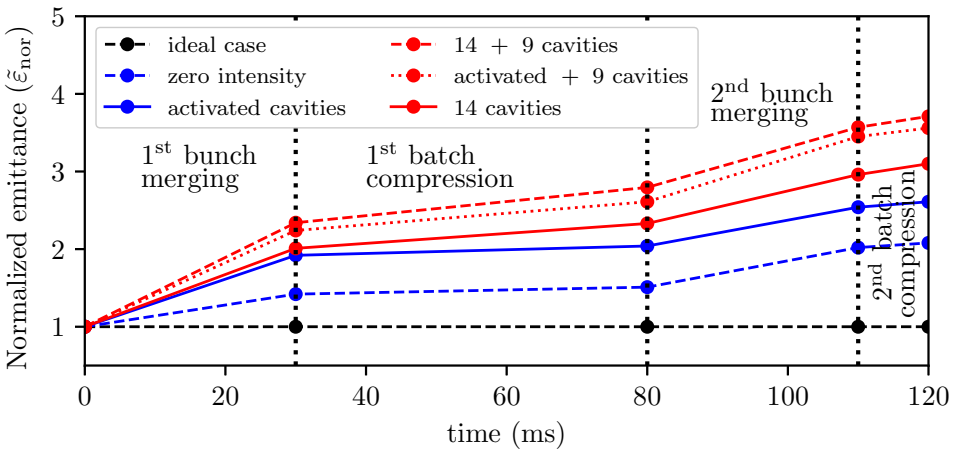

Figure 34: Comparison of the emittance growth at each stage of the heavy ion bunch manipulations. The blue line represents the case in the presence of the beam loading from the activated rf cavities. The red solid line represents the beam loading from the total 14 rf cavities, including both of the activated and the inactivated rf cavities. The red dotted line denotes the beam loading from the activated rf cavities and the 9 compressor cavities. The red dashed line represents the "worst case", which include the total 14 rf cavities and the 9 compression rf cavities. The dashed black line indicates the ideal case.

Table 14: Final parameters of the heavy ion bunch after fast bunch rotation with different beam loading effects in Fig. 34

Parameter [unit]	ideal	zero intensity	activated	total 14	14+9	activated+9
particle percentage	100%	95%	81%	75%	63%	72%
(2σ) bunch length [ns]	55	73	84	92	102	97

10 Summary

The longitudinal manipulations of high-intensity proton and heavy ion beams, including bunch merging, bunch batch compression and fast bunch rotation, in the presence of intensity effect (the longitudinal space charge and cavity beam loading) are theoretically analyzed. The methods to dampen the intensity effects and to optimize the parameter settings in these longitudinal bunch manipulations are presented. As an application of these scheme, an example scenario of longitudinal manipulation of high-intensity proton beams in FAIR SIS100 are proposed and investigated via PIC simulations. It is shown that the emittance growth due to beam loading and space charge can be largely reduced in the presence of the proposed optimization schemes, and the relevant longitudinal parameters for bunch merging and batch compression are also given. Furthermore, some physical mechanism of intensity effect on the longitudinal manipulation, such as the beam loading matching and the beam load damping effect on the filamentation during bunch rotation needs further theoretical study.

Appendix

A Transverse tune shifts

The transverse tune shifts can be evaluated via (see, for example, in Ref. [22])

$$\Delta\nu_x = -\frac{2r_0 I g_f L}{Aqc(\beta c)^3}\frac{2}{\epsilon_x + \sqrt{\epsilon_x\epsilon_y}}, \tag{54}$$

in which r_0 is the classical proton radius, g_f is the factor. For a Gaussian transverse distribution, $g_f = 2.0$, A and q is the mass number and the elementary charge, respectively. I is the beam current, and can be obtained via

$$I = \frac{h}{n_b}\frac{b_f \beta c N Z q}{L} \tag{55}$$

with n_b is the number of bunches in the ring, b_f the bunching factor, Zq the charge of the particle. It can be seen from Eq. 55 that for a bunch merging with constant bunching factor b_f from h_{10} to h_5, and both h and h_b and halved, the current stays constant, causing a constant transverse tune shift.

B Proton bunch manipulation with Gaussian distribution

For a more realistic case, here we investigate the proton bunch manipulation in the presence of space charge and beam loading with initial Gaussian distribution, truncated by 3σ. The simulation are performed with the proposed schemes in Sec. 8.

The simulation results of the particle distribution and the emittance growth are shown in Fig. 35 and Fig. 36 respectively. It can be seen that the emittance growth due to high intensity is smaller than the parabolic distribution. The compensation scheme based on the elliptical model can be well applied for the bunches with Gaussian distribution. We attribute the lower emittance growth in the Gaussian distribution to the Landau damping mechanism, which needs further study.

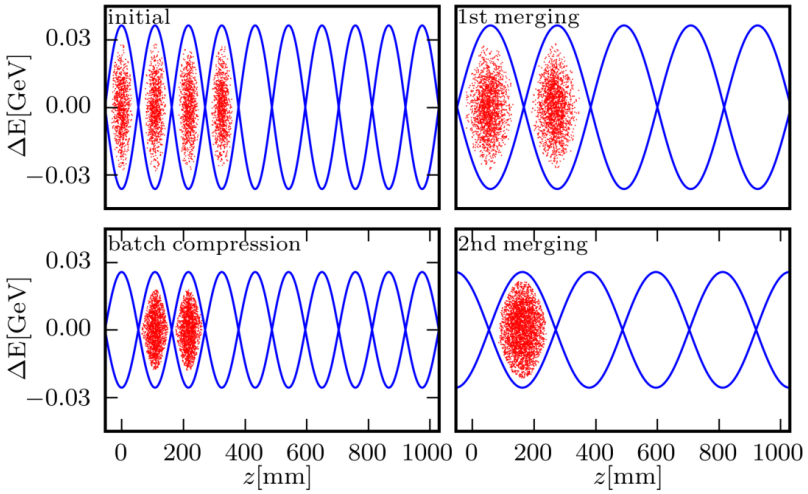

Figure 35: Particle distribution in the longitudinal phase space during proton bunch manipulation with initial Gaussian distribution, in the presence of space charge and beam loading.

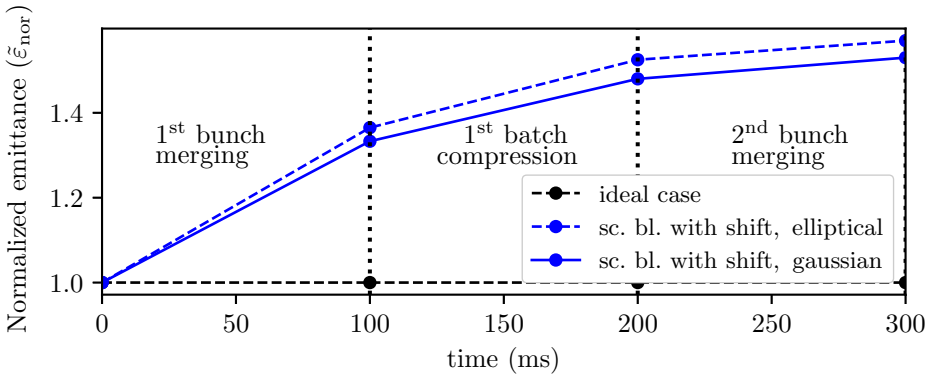

Figure 36: The normalized longitudinal emittance at each stage of the proton bunch manipulation with initial Gaussian distribution in the presence of space charge and beam loading (solid blue line), compared with the case with parabolic distribution (dashed blue line). The ideal case is shown by the black line.

C Proton bunch manipulation starting with $h = 5$

In the section we investigate the longitudinal manipulation of proton bunch starting with $h = 5$. It consists of 4 steps: the first batch compression, the first bunch merging, the second batch compression and the second bunch merging, as schematically shown in Fig 37.

The proposed voltage ramps are shown in Fig. 38. Simulation shows that the oscillation of the during first compression of the 4-bunch-batch is larger than that in the second compression of the 2-bunch batch. Therefore, a longer time of 120 ms is adopted for the first batch compression.

The simulation results of the emittance growth in the presence of the beam loading effects contributed by the working cavities and the total cavities are shown in Fig. 38. The parking harmonics for the inactivated rf cavities is chose to be at $h = 8$.

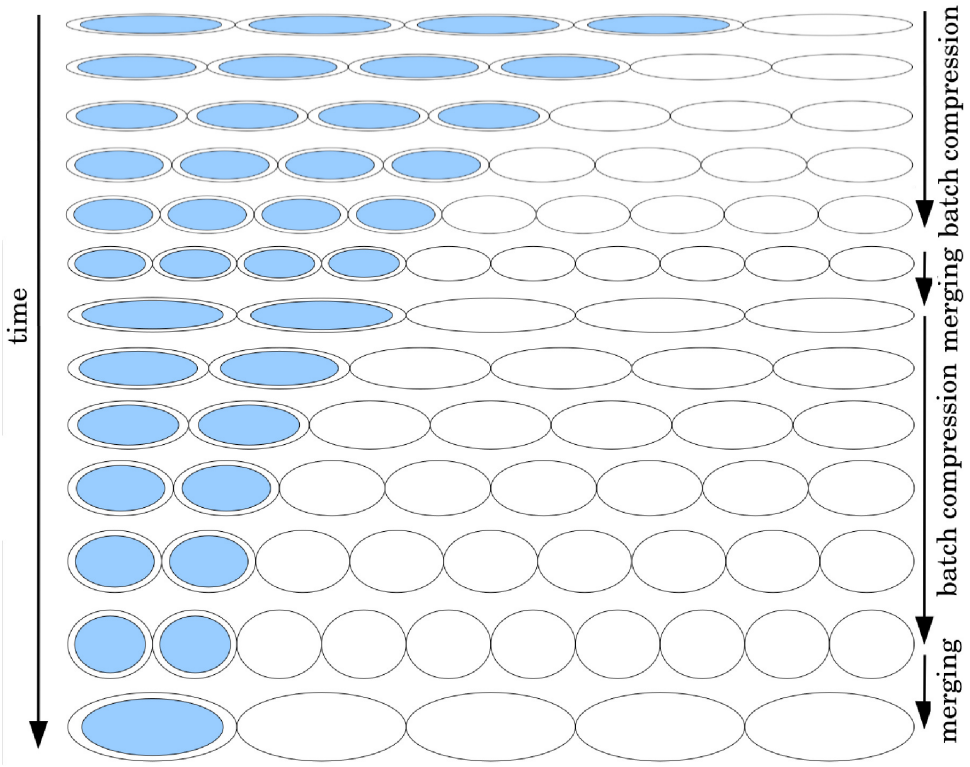

Figure 37: Schematically drawing of the longitudinal manipulation of proton bunch starting with 5 harmonics.

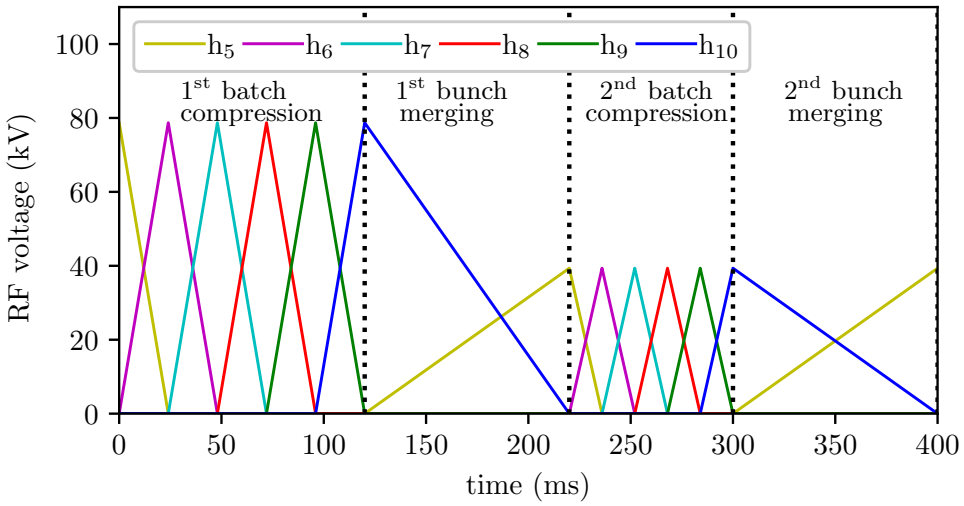

Figure 38: The rf voltage ramps for the longitudinal manipulation of proton bunch starting with $h = 5$.

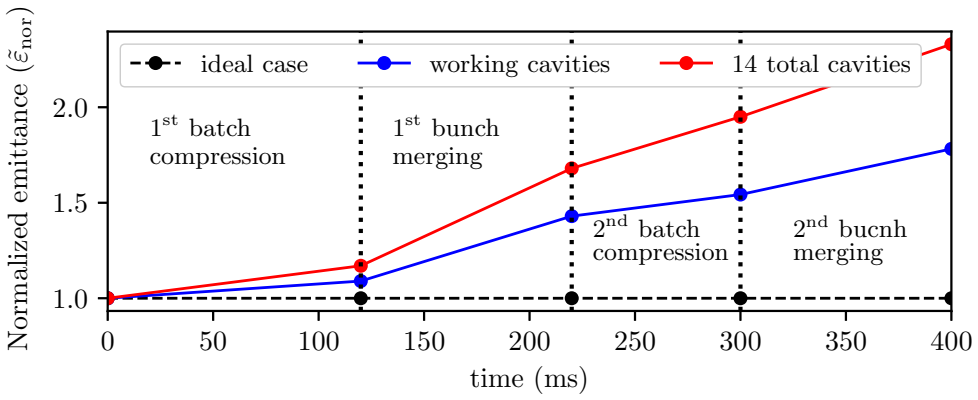

Figure 39: The emittance growth at each stage of the proton bunch manipulations starting with $h = 5$. The blue line represents the case in the presence of the beam loading from the activated rf cavities; while the red line the beam loading from both of the activated and the inactivated rf cavities.

D Bunch merging with shifted-X voltage-ramping scheme

In the section we will compare the proton bunch merging under three different voltage ramping schemes. As shown in Fig. 40, the blue lines represent the voltage ramping scheme employed in the previous example (named "X-ramping" in the following). The green lines and red lines denote two other ramping, named as "shifted-X-ramping" and "doubled-shifted-X-ramping" respectively. The parameters listed in Tab. 3 is adopted in the simulation.

The simulation results of the final emittance after bunch merging are listed in Fig. 41. It can be seen that in the absence of intensity effects (blue in Fig. 41), bunch merging with the doubled-X-ramping scheme has the minimum final emittance. The emittance growth with the X-ramping is slightly larger than that with the X-ramping. This is because the ramping slope is larger, as shown in green curve in Fig. 40.

In the presence of intensity effects, the emittance growth is smallest with the scheme of X-ramping. The bunch merging with the doubled-shifted-X has the largest emittance growth, since it has a longer time under beam loading effects.

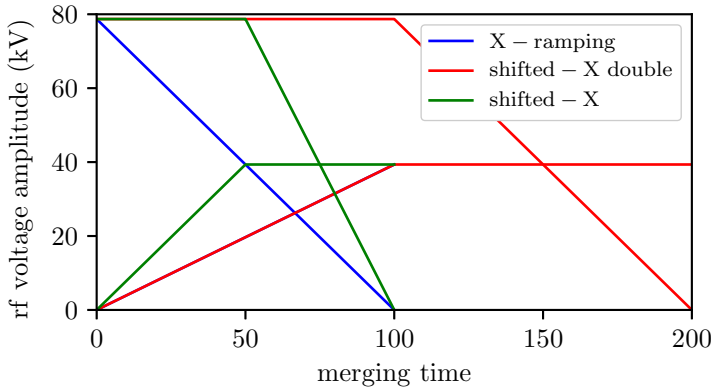

Figure 40: Comparison of three voltage ramping schemes.

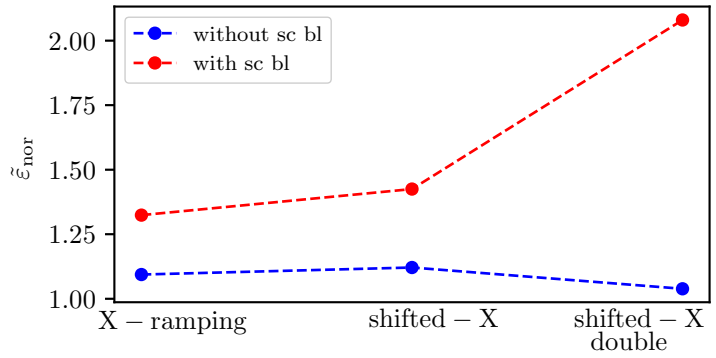

Figure 41: Simulation results of the final normalized emittance after bunch merging with the schemes of the X-ramping, shifted-X ramping and the doubled shifted-X.

References

[1] P. Spiller et al., Status of the FAIR Heavy Ion Synchrotron Project SIS100, in Proceedings of IPAC2015, Richmond, VA, U.S.A., 2015, p. 3715

[2] P. Spiller et al., Status of the FAIR Project, in Proceedings of IPAC2018, Vancouver, Canada, 2018, p. 63

[3] V. Kornilov et al., Beam quality and beam loss predictions with space charge for SIS100, J. Instrum. 15, P07020 (2020).

[4] Yao-Shuo Yuan, Oliver Boine-Frankenheim and Ingo Hofmann, Intensity limitations due to space charge for bunch compression in synchrotrons, Phys. Rev. Accel. Beams **21**, 074201 (2018).

[5] R. Garoby, Bunch merging and splitting techniques in the injectors for high energy hadron colliders. No. CERN-PS-98-048-RF. 1998.

[6] Bozsik, I., et al. Numerical investigation of bunch-merging in a heavy-ion-synchrotron, in *Computing in Accelerator Design and Operation.* Springer, Berlin, Heidelberg, 1984. 128-133.

[7] R. Garoby, New RF Exercises envisaged in the CERN PS for the Antiproton Production Beam of the ACOL Machine, in *Proceedings of the 1985 Particle Accelerator Conference, IEEE, Vancouver, Canada*, p.2332

[8] J. M. Brennan, RF Issues in Booster/AGS/RHIC, in *Proceedings of the Third ICFA Mini-Workshop on High Intensity, High Brightness Hadron Accelerators, BNL-64754 (Informal Report) 1997 May*

[9] L. Ahrens *et al.*, The RHIC Injector Accelerator Configurations, and Performance for the RHIC 2003 Au-d Physics Run, in *Proceedings of the 2003 Particle Accelerator Conference*, IEEE, Portland, USA, 2003.

[10] R. Garoby, RF gymnastics in synchrotrons, in *CERN Yellow Report: CERN-2011-007* (Ed. R Bailey, Geneva, 2012) p. 431.

[11] H. Damerau. Creation and Storage of Long and Flat Bunches in the LHC. PhD thesis, Technische Universität Darmstadt, 2005.

[12] K. Y. Ng, *Physics of intensity dependent beam instabilities*, (World Scientific, Singapore, 2006).

[13] S. Y. Lee, *Accelerator Physics* 3rd ed. (World Scientific, Singapore, 2011).

[14] Martin Reiser, *Theory and design of charged particle beams*, 2nd ed. (WILEY-VCH Verlag GmbH Co. KGaA, Weinheim, 2008)

[15] A. Hofmann and F. Pedersen, Bunches with local elliptical energy distributions, IEEE Trans. Nucl. Sci. 26, 3526 (1979).

[16] O. Boine-Frankenheim and T. Shukla, Space charge effects in bunches for different rf wave forms, Phys. Rev. ST Accel. Beams 8, 034201 (2005).

[17] A. Shishlo, S. Cousineau, V. Danilov, J. Galambos, S. Henderson, J. Holmes and M. Plum, in *Proceedings of the 2006 International Computational Accelerator Physics Conference*, (Chamonix Mont-Blanc, France, 2006), p. 53-58; https://sourceforge.net/projects/py-orbit.

[18] A. Shishlo, S. Cousineau, J. Holmes, T. Gorlov, Procedia Comput. Sci. **51** (2015) 1272–1281.1

[19] A. Chao and M. Tigner, *Handbook of Accelerator Physics and Engineering* 2nd ed. (World Scientific, River Edge, NJ, 2013).

[20] Harald Klingbeil, Ulrich Laier and Dieter Lens, *Theoretical Foundations of Synchrotron and Storage Ring RF Systems*, (Springer, 2015)

[21] PhD Thesis *Beam Loading Effect and Adiabatic Capture in SIS-18 at GSI*

[22] K. Schindl, *Space Charge*, CERN Accelerator School 2003: Intermediate Course on Accelerators, CERN2006-002 (2006).